## **Modeling Report**

# Simulated Rupture of a Carbon Dioxide Pipeline **Near Sorrento Primary School / Orange Grove Subdivision** in Ascension Parish, Louisiana

**Numerical Modeling Using Computational Fluid Dynamics** Five- and Ten-Minute Valve Shutoff Scenario

> DJMG LLC John Gorman, PhD 1554 Asbury St. N St. Paul, MN 55108-2336 Consultant for Earthjustice

> > November 10, 2025 V 2.0

#### EXECUTIVE SUMMARY

Air Products Blue Energy LLC is proposing to construct a pipeline to transport highly pressurized carbon dioxide (CO<sub>2</sub>) from its planned hydrogen and ammonia manufacturing facility in Ascension Parish, Louisiana, to a carbon sequestration facility approximately 38 miles away in Lake Maurepas. The proposed 24-inch diameter pipeline would run approximately one-half mile from the Sorrento Primary School and closer to the Orange Grove Subdivision that is between the school and the pipeline.

A model was created to simulate a sudden rupture of a high-pressure 24-inch CO<sub>2</sub> pipeline near the Sorrento Primary School and Orange Grove Subdivision using the same pipeline route and basic construction parameters (e.g., pipeline dimensions, pipeline depth, shutoff valve locations, etc.) as that proposed by Air Products. The model assumes the pipeline valve will fully close either five or ten minutes after the rupture is detected, Case 1 and Case 2, respectively. The longer the valve shut-off time, the more CO<sub>2</sub> will be released. The five-minute timeframe was used here to reflect industry goals, but a real-world scenario would likely take longer. The ten-minute scenario was also modeled to provide a more realistic valve shutoff time, although the actual shutoff time could exceed ten minutes.

Even with these optimistic closure scenarios, the simulation results show the rupture would cause the release of a large amount of CO<sub>2</sub> that would reach the subdivision and school at concentrations of 50,000 ppm (or 5 percent) for about 10 minutes, which exceeds the short-term exposure limit of 30,000 ppm (or 3 percent) for 10 minutes, and is above the National Institute for Occupational Safety and Health's (NIOSH) Immediately Dangerous to Life and Health (IDLH) value of 40,000 ppm (Table 1). Symptoms above 30,000 ppm include shortness of breath, dizziness, and increased heart rate and blood pressure. In the case of the ten-minute valve shutoff time, more CO<sub>2</sub> was released as a result of the pipe rupture compared to the five-minute valve closure time. The simulation results for the longer shut-off time also showed an increase in the predicted cumulative CO<sub>2</sub> exposure times in regions further downstream from the rupture in the subdivision and school area.

#### HEALTH EFFECTS FROM EXPOSURE TO HIGH CO<sub>2</sub> CONCENTRATIONS

The health effects due to CO<sub>2</sub> inhalation can vary greatly, even in healthy individuals, depending on the concentration and duration (length of time) someone is exposed. While the symptoms due to CO<sub>2</sub> inhalation vary, according to [1], possible symptoms at different concentrations are included in Table 1.

Table 1. Potential health effects from exposure to different CO<sub>2</sub> concentrations [1].

Concentration	Potential health effects	
5,000 ppm (0.5%)	OSHA Permissible Exposure Limit (PEL) and ACGIH Threshold	
	Limit Value (TLV) for 8-hour exposure	
10,000 ppm (1.0%)	Typically no effects, possible drowsiness	
15,000 ppm (1.5%)	Mild respiratory stimulation for some people	
30,000 ppm (3.0%)	Moderate respiratory stimulation, increased heart rate and bloo	
	pressure, ACGIH TLV-Short Term	
40,000 ppm (4.0%)	Immediately Dangerous to Life or Health (IDLH)	
50,000 ppm (5.0%)	Strong respiratory stimulation, dizziness, confusion, headache,	
	shortness of breath	
80,000 ppm (8.0%)	Dimmed sight, sweating, tremor, unconsciousness, and possible	
	death	

(Note that for well-ventilated places, such as a home or office, the typical ppm of  $CO_2$  in the air is in the range of 400 to 1,000 ppm or 0.04% to 0.1%.)

#### **MODELING OVERVIEW**

In order to conduct a comprehensive analysis of a CO<sub>2</sub> pipeline rupture, information is needed across several key areas: the pipeline's characteristics, the conditions of the rupture, the properties of the CO<sub>2</sub> being transported, and the surrounding environment. The necessary information can be broken down further:

- **Pipeline Design:** The pipeline's specifications, including diameter, length, distances between shutoff valves, and the depth it is buried.
- **Operating conditions:** The pressure and temperature inside the pipeline just before the rupture occurred.

- Leak detection: Information on the pipeline's leak detection system, specifically the time needed to detect a leak/rupture.
- **Isolation procedures:** Data on the effectiveness and time required to shut the valves and isolate the affected pipeline segment.
- Type of rupture: The specific cause of the rupture, such as corrosion, mechanical failure (e.g., weld issues), third-party damage, or stress from ground movement. The size and type of the rupture (e.g., pinhole leak, full-bore rupture, zipper-like fracture, guillotine cut, etc.), which affects the CO<sub>2</sub> release rate and energy.
- Transported product: The exact composition of the CO<sub>2</sub> stream, including the percentage of CO<sub>2</sub> and any impurities.
- Location: The precise location of the rupture, including geographic coordinates, proximity to infrastructure, and details on surrounding topography. The surrounding topography could trap or channel the heavier-than-air CO<sub>2</sub> cloud.
- Meteorological conditions: Wind speed and direction, temperature, and atmospheric stability at the time of the rupture. This is critical because CO<sub>2</sub> is heavier than air and its dispersion is highly influenced by weather.

The results from a comprehensive analysis of a CO<sub>2</sub> pipeline rupture can aid in determining potential hazard zones where the CO<sub>2</sub> spreads (referred to as plumes or clouds), preparing emergency response protocols, assessing the impact on evacuation and emergency responses, and assessing the damage to surrounding vegetation and animal life.

There are two common methods for numerically predicting CO<sub>2</sub> plume concentrations and impact zones: dispersion modeling and computational fluid dynamics (CFD). The first approach, dispersion modeling, is a method based on simplified diffusion zones with uniform or assumed concentration profiles that move in the direction of the prevailing wind. Dispersion modeling, because of its relative simplicity, has been more commonly used for CO<sub>2</sub> plume modeling. The other approach, CFD, is a technique that solves the governing equations (conservation of mass, momentum, and energy) at millions of calculation points. While performing CFD simulations are more complex and requires greater computational resources and time, the results are considered

more accurate because they can account for complexities such as topography, various weather conditions, and more. CFD modeling was employed here.

#### SIMULATION INPUT PARAMETERS

For the current numerical simulation, a CO<sub>2</sub> pipeline (24-inch outer diameter) as proposed by Air Products (p. 7 in [2]) experiences a sudden guillotine cut in a 5.8-mile long section of the pipeline between the Air Products' planned facility (where the CO<sub>2</sub> is generated) and the location of the first shutoff valve (p. 24 in [2]). The pipe is buried three feet below the ground, which is the minimum depth for most locations of the onshore portion of Air Products' proposed pipeline (p. 14 in [2]). A guillotine cut in the modeled pipeline is located approximately 1.5 miles along the Air Products' proposed pipeline route from the planned facility (Figure 1-2 on p. 9 in [2]).

A "guillotine cut" in a pipeline refers to a catastrophic rupture where the pipe breaks completely across its diameter, as if sliced cleanly in two. This type of instantaneous rupture can be caused by a combination of factors, such as corrosion, metal fatigue, bending due to soil settlement, ground movement, external damage, or flaws in welds compounded by thermal or mechanical stresses. The guillotine cut pipeline rupture is similar to the type of CO<sub>2</sub> rupture that occurred near the town of Satartia, Mississippi, USA, on February 22, 2020 [3], involving a 9.55-mile, 24-inch diameter pipeline.

Once the pipe ruptures, the pure CO<sub>2</sub>, which is flowing in the pipeline as a high-pressure, densephase liquid, emerges from the rupture and changes phase to become primarily gaseous in the ambient atmosphere. At the rupture, the high-pressure CO<sub>2</sub> experiences many complex physical phenomena such as rapid expansion, the Joule-Thomson effect, phase change, and choked flow, all of which impact the dispersion of the resulting CO<sub>2</sub> plume.

The parameters chosen for the simulation are listed in Table 2. The pipeline parameters (pressure, temperature, and shutoff time) were estimated because the actual parameters were not provided by Air Products.

Table 2: Simulation parameters.

Parameter	English units	Metric units	
Ambient air pressure	14.7 psi	101.325 kPa	
Ambient temperature	68 °F	20 °C	
Wind speed $(U_{I\theta})$	4.3 mph	1.92 m/s	
Wind direction	South		
Initial CO <sub>2</sub> pipeline pressure	2,200 psig	15,168 kPa	
Initial CO <sub>2</sub> pipeline temperature	50 °F	10 °C	
Shutoff time (to close valves)	5 or 10 minutes		

In Table 2, the wind speed  $(U_{10})$ , represents the wind velocity measured at a height of 10 meters from the ground, corresponding to an atmospheric boundary layer velocity profile at the solution domain's southern boundary. The wind speed is constant before and during the pipe rupture. The average air temperature, wind speed, and direction are from meteorological data retrieved from [4]. (Note: The meteorological convention for wind direction is to state the direction from which the wind originates.)

The initial CO<sub>2</sub> pipeline pressure represents the pressure in the pipeline just prior to the rupture; once the pipeline ruptures, the pressure drops and varies with time and position as the CO<sub>2</sub> exits the pipe. According to the Air Products Blue Energy LLC Joint Permit Application, 1-2-1 CO2 Pipeline Alignment Sheets, the maximum allowable pressure in the pipeline is 2,200 psig, so that pressure was used as the initial CO<sub>2</sub> pressure.

Under normal operating conditions, as the CO<sub>2</sub> is transported/piped over long distances underground, it is expected to reach thermal equilibrium with the ground eventually. The initial CO<sub>2</sub> pipeline temperature listed in Table 2 represents the CO<sub>2</sub> temperature before a potential rupture occurs, corresponding to an assumed ambient temperature three feet below ground. Once a rupture occurs, the situation changes drastically. The CO<sub>2</sub> temperature varies over time both inside and outside of the pipeline as it rapidly expands from the rupture point. This expansion causes a significant cooling effect, drastically lowering the temperature of the CO<sub>2</sub> as it escapes into the atmosphere.

For the purposes of the simulation, it is assumed that the rupture is detected, and the valves are closed either five or ten minutes after the rupture occurs, in Cases 1 and 2, respectively. The shutoff time of 5 minutes reflects industry goals for automatic valves, but is likely an optimistic response timeframe. The time allowed by the Pipeline and Hazardous Materials Safety Administration (PHMSA) regulations in [5] requires CO<sub>2</sub> pipelines with ruptures to be isolated by valves within 30 minutes or less. However, the National Transportation Safety Board (NTSB) has recommended shorter response times to PHMSA; as seen in [6], the NTSB referenced an operator's claim of a 5to-10-minute notification time after identifying a rupture. For reference, in the Satartia, Mississippi rupture, according to [3], the rupture was detected, and the valves were closed in 8 minutes. Once the pipeline valves close, the remaining CO<sub>2</sub> in the isolated section of the pipeline exits through the rupture until the pipeline is empty.

The results are highly sensitive to the operating conditions of the pipeline, which can significantly impact the results of a CO<sub>2</sub> pipeline rupture analysis, the level of hazard, the area of impact, and the resulting concentrations.

The overall numerical solution domains for the Sorrento Primary School and the residential homes in the Orange Grove Subdivision are shown in Figure 1.

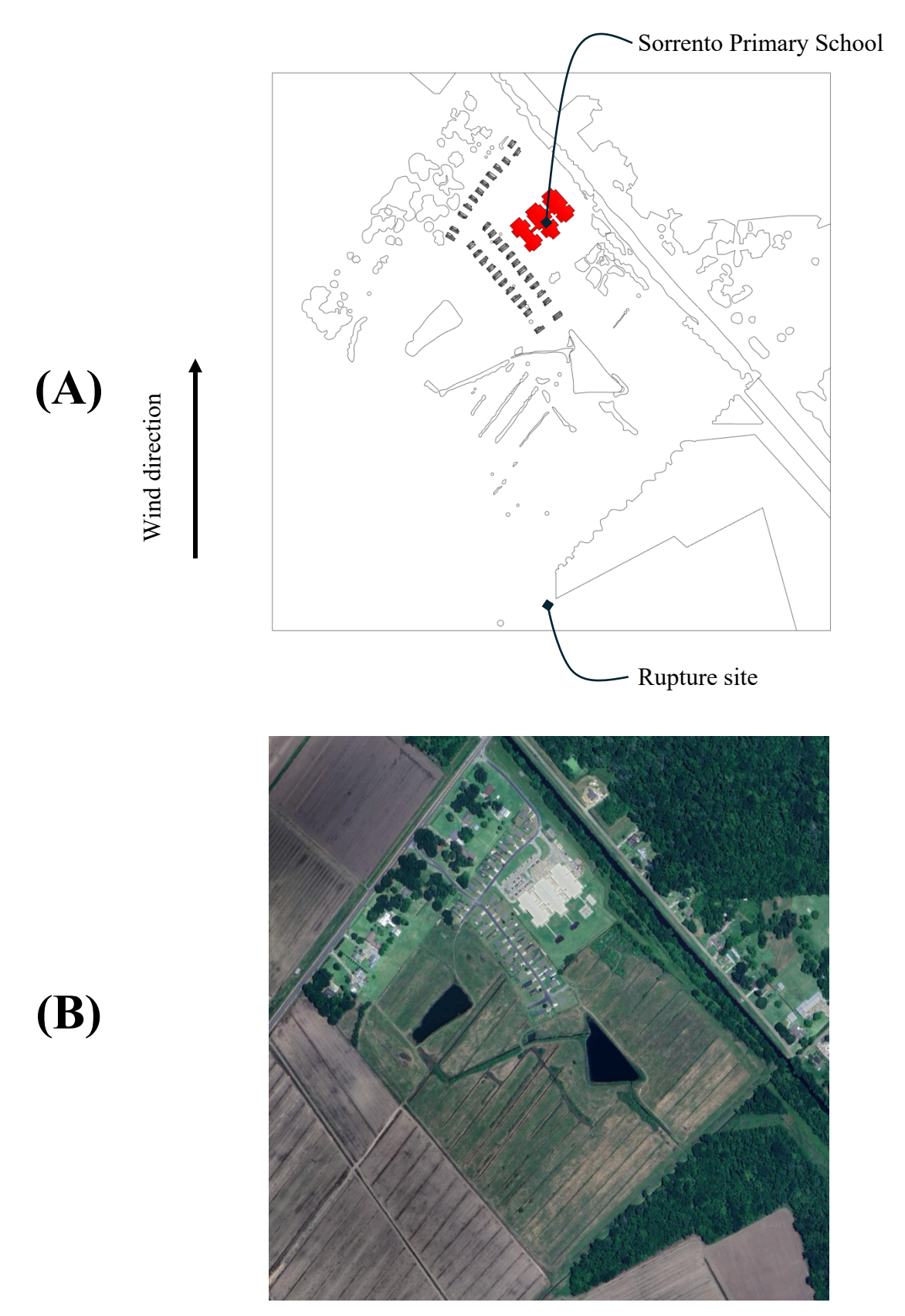


Figure 1. Comparison of (A) Numerical Solution Domain and (B) Geographic Map [7] for Sorrento Primary School and Orange Grove Subdivision area.

The solution domain (numerical model) for the Sorrento Primary School and Orange Grove Subdivision area, seen in Figure 1, is approximately 4,000 ft in the wind flow direction, 4,000 ft wide, and 400 ft in the vertical direction. Upstream of the pipe rupture (south), an inlet atmosphere wind velocity profile is used, while the sides, top, and downstream boundaries of the solution domain were treated as openings with entrainment at atmospheric conditions.

#### **NUMERICAL MODELING**

The numerical approach and modeling process employed here will be similar to the approach presented in [8]. In [8], it was shown that numerical modeling using computational fluid dynamics is able to accurately simulate real-world CO<sub>2</sub> ruptures. Specifically, [8] had good agreement between the CFD model and the CO<sub>2</sub> pipeline rupture that occurred near Satartia, Mississippi, USA, on February 22, 2020. This is particularly relevant since the CO<sub>2</sub> pipeline near Satartia is similar in size to the proposed Air Products pipeline being analyzed here.

#### Governing equations

The simulations will make use of the Reynolds-Averaged Navier-Stokes (RANS) equations, in conjunction with an appropriate turbulence model. Here, it was chosen to use the Shear Stress Transport (SST)  $\kappa$ - $\omega$  turbulence model [9, 10] since it has been repeatedly shown to give good agreement with a wide range of experimental comparisons [11–19]. The SST model is a blending of two different but well-known turbulence models, respectively, the  $\kappa$ - $\omega$  and  $\kappa$ - $\varepsilon$  models.

These numerical models, based on computational fluid dynamics (CFD), rely upon the simultaneous solution of fundamental equations throughout the solution domain: conservation of mass, momentum, concentration, and energy. When multiple species are involved, the bulk motion of the mixture is solved using singular values of pressure, temperature, and velocity; however, each species has its own separate conservation of mass. In this study, there are two species (air and carbon dioxide). While air is a mixture, primarily of Nitrogen (N<sub>2</sub>) and Oxygen (O<sub>2</sub>), it is standard to treat it as a single species with properties that reflect the mixture. For air, the fluid material

properties are determined by the ideal gas law, and for carbon dioxide (CO<sub>2</sub>) in the supercritical, liquid, or gas phase, the Peng Robinson equation of state was used.

The conservation of mass for species i is expressed as

$$\frac{\partial \rho_i}{\partial t} + \frac{\partial (\rho_i u_j)}{\partial x_j} = -\frac{\partial (\rho_i (u_{ij} - u_j) - \overline{\rho_i u_j})}{\partial x_j} \tag{1}$$

In this equation,  $r_i$  is the mass-average density of the  $i^{th}$  fluid component in the mixture; the subscript i refers to the  $i^{th}$  component, and the subscript j refers to a tensor direction. The  $u_j$  term is the mass-average velocity in the j direction. Equation 1, when applied to both components in the mixture, becomes

$$\frac{\partial \rho_i}{\partial t} + \frac{\partial (\rho_i u_j)}{\partial x_i} = 0 \tag{2}$$

The relative motion of the two species may be different because of diffusion effects (driven by concentration gradients), and the governing diffusion equation is

$$\rho_i \left( u_{ij} - u_j \right) = D_i \frac{\partial(\rho_i)}{\partial x_i} \tag{3}$$

The symbol  $D_i$  is the kinematic diffusivity of species i. The multi-component specific equations of concentration are solved as a scalar transport equation with the mass fraction f as the variable. The resulting transport equation is

$$\frac{\partial \rho \phi_i}{\partial t} + \frac{\partial \rho \phi_i u_i}{\partial x_i} = \frac{\partial \left( D_i \frac{\partial \phi_i}{\partial x_j} \right)}{\partial x_i} - \frac{\overline{\partial \rho \phi_i u_i}}{\partial x_i} \tag{4}$$

Differential transport of a species is reproduced using an eddy dissipation approximation with a turbulent Schmidt number so that the species transport equation can be rewritten as

$$\frac{\partial \rho \phi_i}{\partial t} + \frac{\partial \rho \phi_i u_i}{\partial x_j} = \frac{\partial \left( D_{eff} \frac{\partial \phi_i}{\partial x_j} \right)}{\partial x_j} \tag{5}$$

With the term  $D_{eff}$  including both molecular and turbulent diffusion. The other constraint in a multicomponent system is that the sum of all mass fractions must equal 1.

Conservation of momentum is written as

$$\rho\left(\frac{\partial u_j}{\partial t} + u_i \frac{\partial u_j}{\partial x_i}\right) = -\frac{\partial p}{\partial x_i} + \frac{\partial}{\partial x_i} \left( (\mu + \mu_t) \frac{\partial u_j}{\partial x_i} \right) + S_{m,i} \quad j = 1,2,3$$
 (6)

In these equations, x indicates a tensor-based direction, and u represents mixture velocities in the x, y, and z directions. The symbols  $\rho$ ,  $\mu$ , p, and  $\mu_t$  are, respectively, density, molecular viscosity, pressure, and eddy viscosity. The term  $S_{m,i}$  represents the porous media source term. With respect to thermal energy, the governing equation is provided in enthalpy form as

$$\frac{\partial(\rho h)}{\partial t} - \frac{\partial p}{\partial t} + \frac{\partial \rho u_j h}{\partial x_j} = \frac{\partial}{\partial x_j} \left( k \frac{k}{c_p} + \frac{\mu_t}{Pr_{turb}} \right) \frac{\partial h}{\partial x_j}$$
 (7)

Enthalpy terms, h, are mass-weighted averages of the two species. All local fluid properties are calculated using the results from the energy equation. Solutions to the energy equations are essential to quantify the buoyancy effects. The buoyancy model uses the density difference of the fluids.

Turbulence is modeled using the Shear Stress Transport model, which is a two-equation turbulence model based on turbulent kinetic energy (k) and the specific rate of turbulence dissipation (w). The turbulence equations are

$$\frac{\partial(\rho k)}{\partial t} + \frac{\partial(\rho u_i k)}{\partial x_i} = P_k - \beta_1 \rho k \omega + \frac{\partial}{\partial x_i} \left[ \left( \mu + \frac{\mu_{turb}}{\sigma_k} \right) \frac{\partial k}{\partial x_i} \right]$$
 (8)

$$\frac{\partial(\rho\omega)}{\partial t} + \frac{\partial(\rho u_i\omega)}{\partial x_i} = \alpha_3 \frac{\omega}{\kappa} P_{\kappa} - \beta_2 \rho \omega^2 + \frac{\partial}{\partial x_i} \left[ \left( \mu + \frac{\mu_{turb}}{\sigma_{\omega}} \right) \frac{\partial\omega}{\partial x_i} \right] + 2(1 - F_1) \rho \frac{1}{\sigma_{\omega 2} \omega} \frac{\partial k}{\partial x_i} \frac{\partial\omega}{\partial x_i}$$
(9)

and the turbulent viscosity is found from

$$\mu_t = \frac{a\rho k}{max(a\omega, SF_2)} \tag{10}$$

 $P_k$  is the production of turbulent kinetic energy, and w reflects the specific rate of turbulent destruction. As noted earlier, the s terms are turbulent Prandtl numbers associated with their subscript. The function  $F_I$  is the aforementioned blending function that transfers the  $\kappa$ - $\omega$  model near the wall to the  $\kappa$ - $\varepsilon$  model away from the wall from the wall boundary conditions. The S term is the magnitude of the shear strain rate.

## **Boundary conditions**

The inlet wind boundary condition, from the south, was a velocity profile corresponding to an atmospheric boundary layer (ABL). There are multiple profiles and equations in the published literature that purport to provide an algebraic representation of the ABL. The selected algebraic equation describing the ABL velocity profile was taken from [20] and is stated in Equation (11).

$$U(y) = \frac{u_*}{K} \ln \left( \frac{y + y_0}{y_0} \right) \tag{11}$$

In addition to the velocity profile, the turbulence characteristics of the ABL are needed and are given in Equations (12) and (13).

$$\kappa = \frac{u_*^2}{\sqrt{C_\mu}} \tag{12}$$

$$\varepsilon(y) = \frac{u_*^3}{K(y+y_0)} \tag{13}$$

In the foregoing, U(y) is the streamwise velocity at the inlet to the solution domain,  $\kappa$  is the

turbulence kinetic energy,  $\varepsilon(y)$  is the eddy dissipation rate, K is the von Karman constant (0.42), y is the height above ground,  $y_0$  is the surface roughness, and  $C_{\mu}$  is a model constant (0.09). The friction velocity  $u_*$  is defined in Equation (14).

$$u_* = \frac{\kappa \, u_{y\prime}}{\ln\left(\frac{y\prime + y_0}{y_0}\right)} \tag{14}$$

In this equation,  $U_{y'}$  is a specified reference velocity at a height y'. The value of  $y_0$  was taken to be that of grassland ( $y_0 = 0.03$  m), as given in [21]. The calculated velocity profiles in this ABL model are based on reference velocities that occur ten meters from the ground ( $U_{y'} = U_{I0}$ ). The aforementioned ABL equations have been shown to have good agreement with experimental measurements [22]. For the present study,  $U_{I0}$  was set at 1.92 m/s (4.3 mph). It should be noted that even though the inlet velocity is constant, obstructions in the solution domain, such as trees or buildings, cause unsteady air currents.

In addition to the wind inlet and the ground (no slip) boundary condition, the remaining boundaries of the solution domain were specified as *openings* (entrainment) at a gauge pressure of 0 Pa. At the opening boundaries, the specification for turbulence was zero gradient. These 'weak' boundary conditions allowed the air to enter or leave the solution domain, at any velocity or direction, without prescribing or imposing values of turbulence at the opening's boundaries, and ultimately provide more accurate results.

The trees within the solution domain were modeled as a porous media to represent their effect on airflow without resolving the complex geometry of individual leaves and branches. This approach adds a momentum sink term to the flow equations, which creates a drag force proportional to the air velocity squared, effectively slowing the wind and generating turbulence. For a forest canopy in Louisiana, characterized by diverse species such as Bald Cypress, Southern Live Oak, and Sweetgum, a porous medium is ideal. The trees were modeled to have a medium density canopy with a porosity of 50%, and a resistance loss coefficient of 1.0 m<sup>-1</sup>.

## Computational Grid and Convergence

The grid was generated such that the non-dimensional near-wall mesh-quality metric known as y+ near fluid-solid boundary surfaces was sufficiently resolved. For the SST  $\kappa$ - $\omega$  turbulence model, y+ values on the order of 1.0 or less are preferred to achieve the most accurate results. In addition to obtaining appropriate y+ values, a grid independence study using several different computational grids was employed by systematically varying the node count (a node is the location where the calculations are performed). For the Sorrento Primary School solution domain, the grid had ~71 million nodes (~224 million elements).

The solutions were considered to be converged to sufficient accuracy when the root-mean-square (RMS) residuals for all of the governing equations were  $10^{-6}$  or less. The simulations were performed as a transient using time steps of 0.001 seconds to keep the RSM Courant number for all of the simulations at or less than 1.0.

#### CO<sub>2</sub> PIPELINE SIMULATION RESULTS

## Case 1 — 5-minute shutoff time

The numerical model of the CO<sub>2</sub> pipeline rupture (5.8-mile-long section with a 24-inch outer diameter and buried three feet underground) was run, simulating two hours of time after the initial rupture. Exactly five minutes after the rupture began, the pipeline valves (located away from the rupture) were closed, and the remaining CO<sub>2</sub> in the pipeline exited into the atmosphere. The total amount of CO<sub>2</sub> released during the simulated rupture was approximately 18,000 barrels of CO<sub>2</sub> (which is the equivalent pre-rupture volume of pure CO<sub>2</sub> using the 42-gallon barrel, found from knowing the density and mass of CO<sub>2</sub>). As a comparison, approximately 31,400 barrels of CO<sub>2</sub> were reported in [3] to have been released at the rupture near Satartia, Mississippi, from a 9.55-mile length of 24-inch diameter pipeline.

Due to the complexity of the physical situation (time-varying changes in CO<sub>2</sub> concentrations over a large three-dimensional area), the results will be presented using several methods: (1) color

contour figures of the CO<sub>2</sub> plume as it expands, (2) color contour figures showing the exposure times of different CO<sub>2</sub> concentrations over the area, (3) a graph showing the CO<sub>2</sub> concentration as a function time near the location of interest.

## Sorrento Primary School — Color contour images of the CO2 plume

The temporal evolution of the CO<sub>2</sub> plume is captured in a series of qualitative diagrams, shown in Figures 2 to 7. These visualizations illustrate the plume's expansion, instantaneous concentrations (in ppm, *parts per million*), and dispersion patterns at key time intervals following the initial rupture. The figures display concentrations at a height of six feet above the ground. For the areas downstream of the rupture, around the Orange Grove Subdivision and Sorrento Primary School, the CO<sub>2</sub> concentrations three feet above or below (± 3 ft) the six-foot height can vary by up to 6 percent, depending on the time and location. This is worth noting because these results show CO<sub>2</sub> concentrations that are relevant for both adults (approximately 5-6 ft tall) and primary school children (typically between 3.5 to 5 ft tall). For example, at 20 minutes after the rupture, the concentration at a location 2,500 ft directly downstream from the rupture was 34,438 ppm, 33,771 ppm, and 33,192 ppm at heights of three, six, and nine feet, respectively. Generally, since CO<sub>2</sub> gas is denser than air, concentrations are higher closer to the ground.

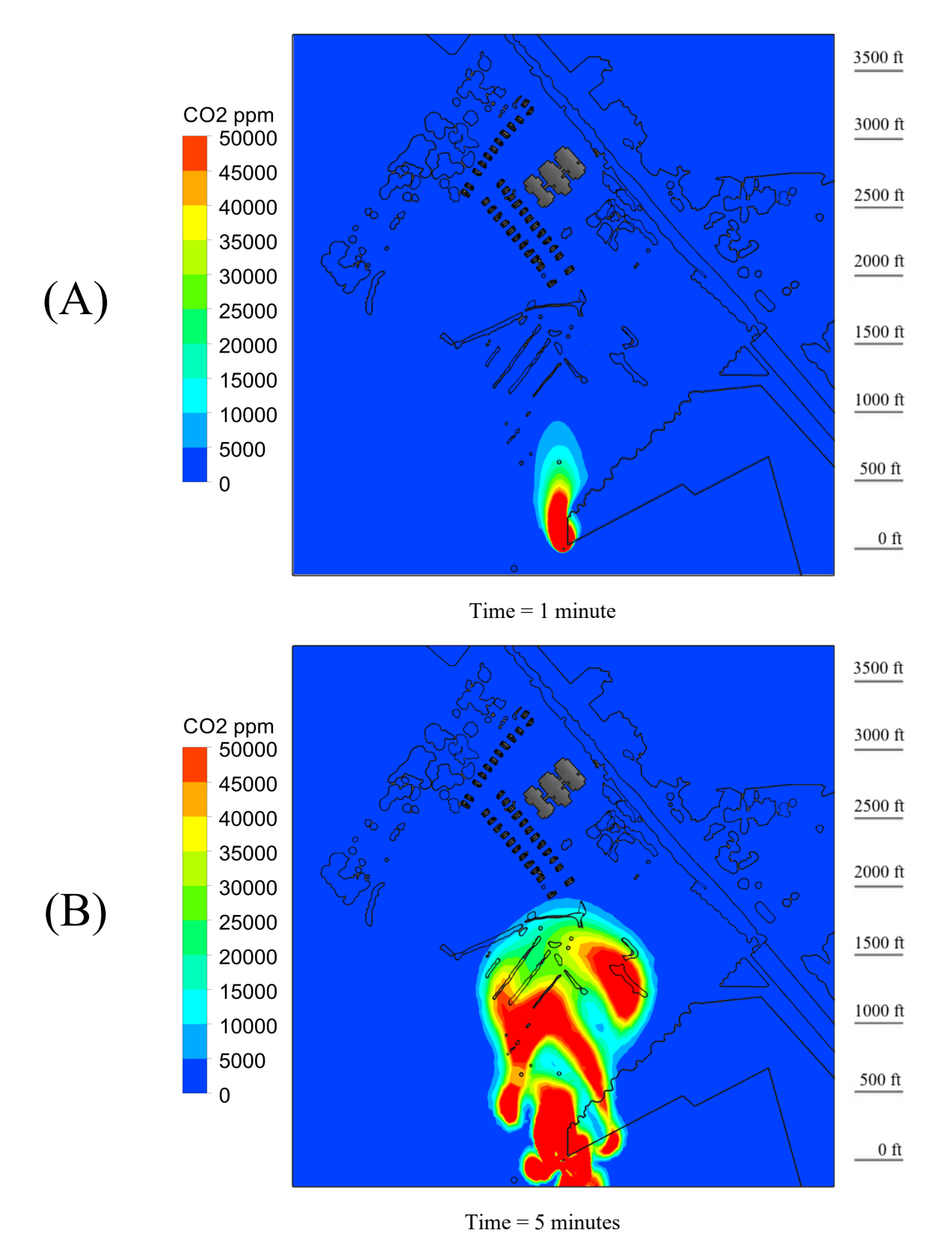


Figure 2. Contour diagrams of instantaneous CO<sub>2</sub> concentrations for the Sorrento Primary School area, 5-minute shutoff time. (A) 1 minute after the rupture and (B) 5 minutes after the rupture.

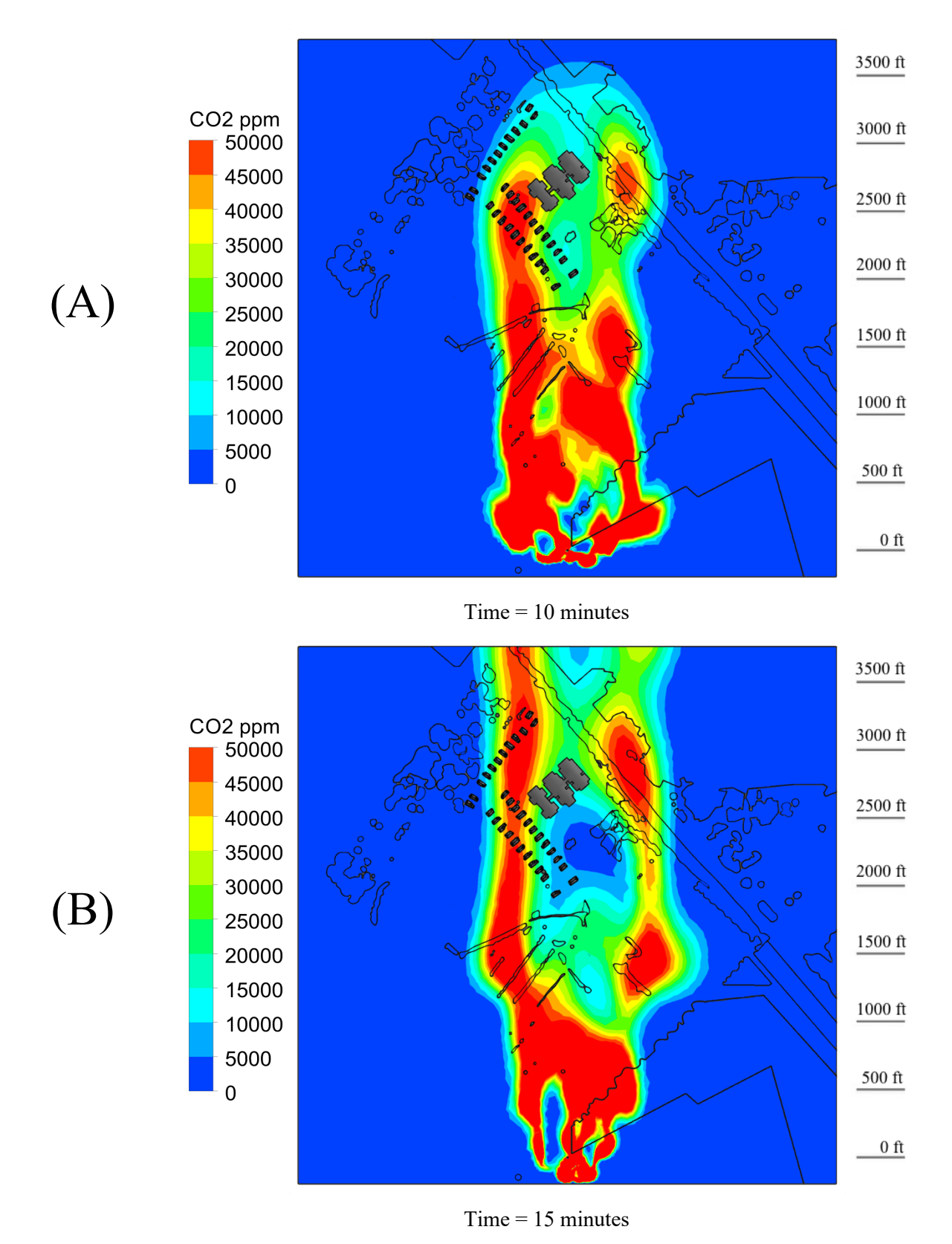


Figure 3. Contour diagrams of instantaneous CO<sub>2</sub> concentrations for the Sorrento Primary School area, 5-minute shutoff time. (A) 10 minutes after the rupture and (B) 15 minutes after the rupture.

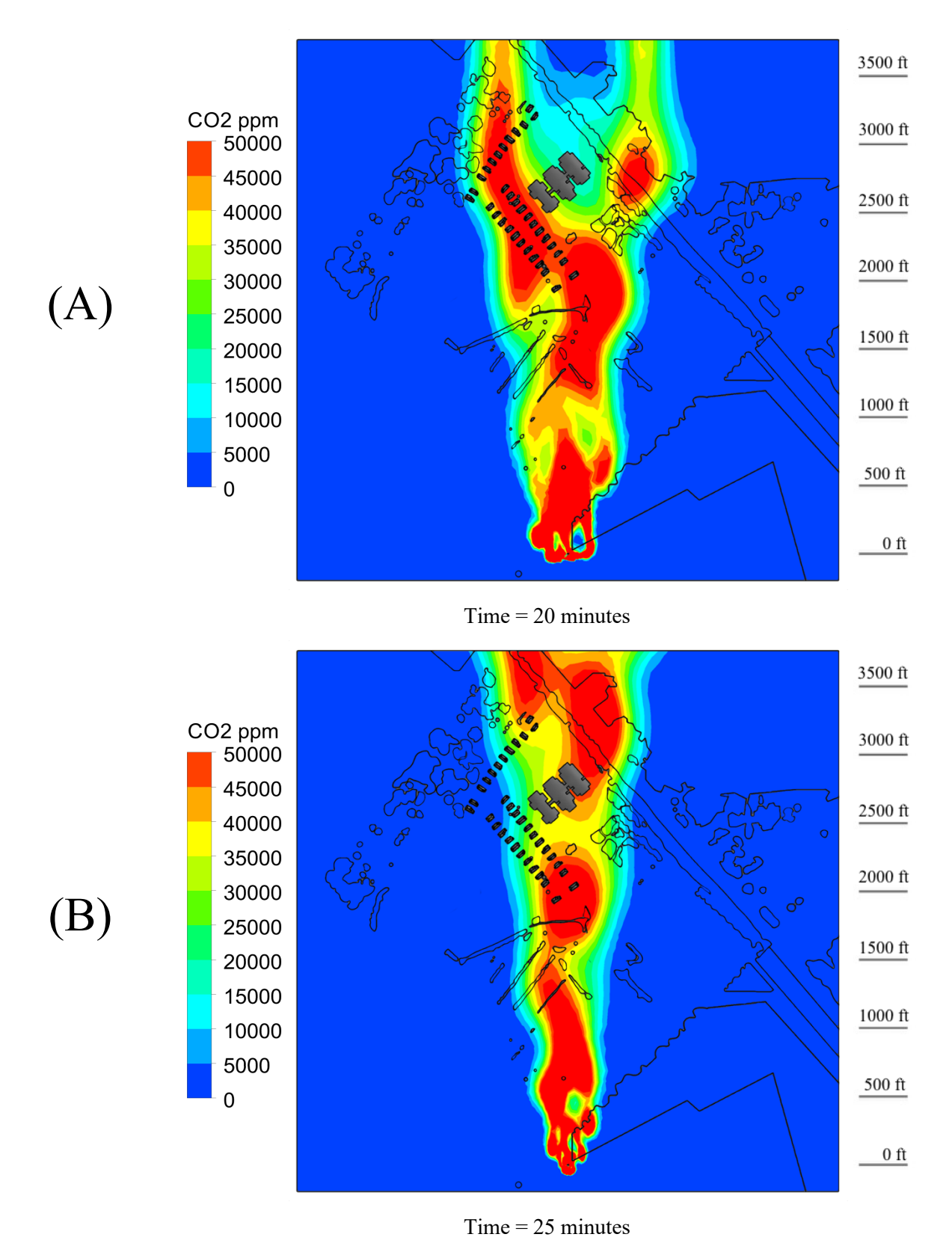


Figure 4. Contour diagrams of instantaneous CO<sub>2</sub> concentrations for the Sorrento Primary School area, 5-minute shutoff time. (A) 20 minutes after the rupture and (B) 25 minutes after the rupture.

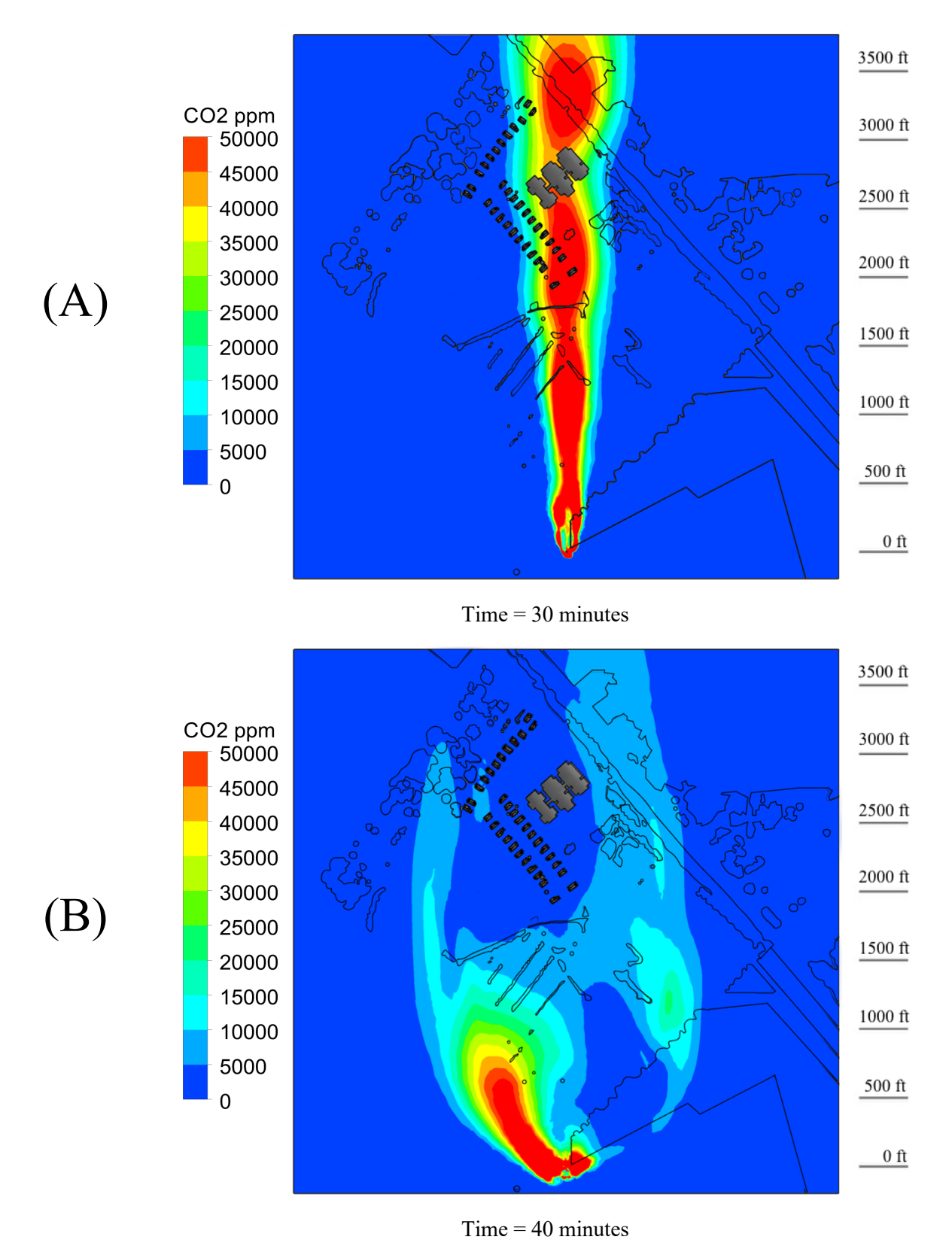


Figure 5. Contour diagrams of instantaneous CO<sub>2</sub> concentrations for the Sorrento Primary School area, 5-minute shutoff time. (A) 30 minutes after the rupture and (B) 40 minutes after the rupture.

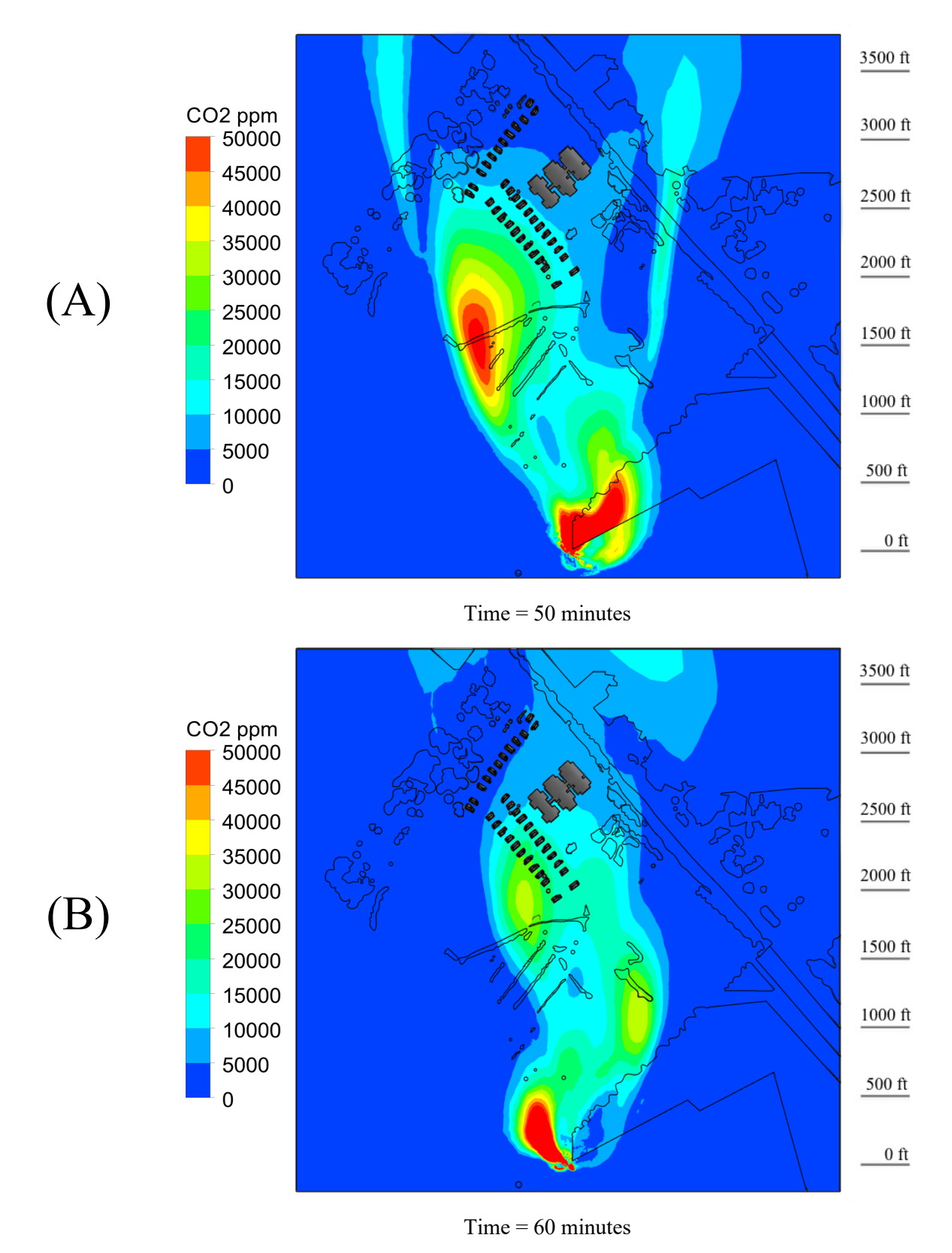


Figure 6. Contour diagrams of instantaneous CO<sub>2</sub> concentrations for the Sorrento Primary School area, 5-minute shutoff time. (A) 50 minutes after the rupture and (B) 60 minutes after the rupture.

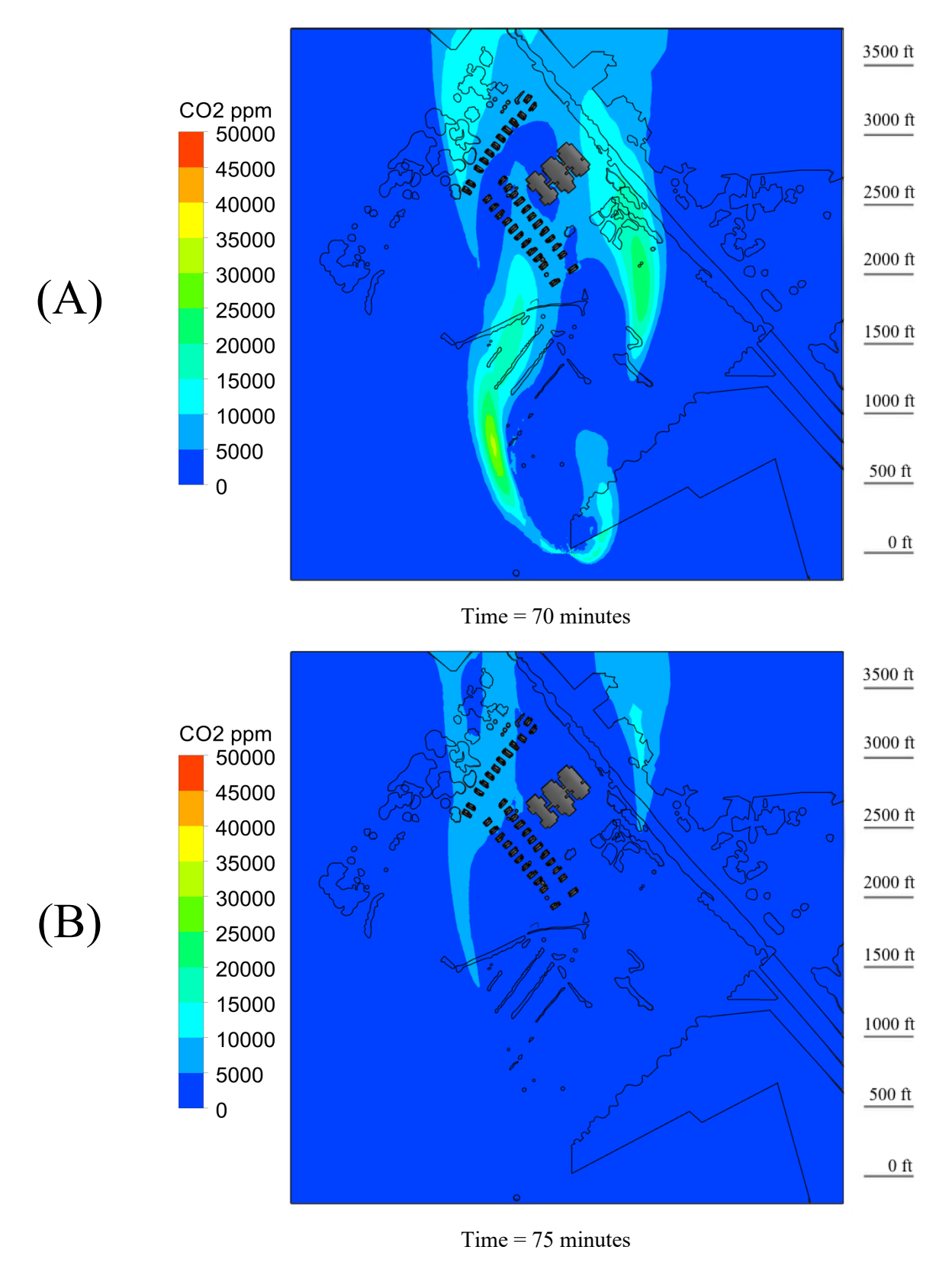


Figure 7. Contour diagrams of instantaneous CO<sub>2</sub> concentrations for the Sorrento Primary School area, 5-minute shutoff time. (A) 70 minutes after the rupture and (B) 75 minutes after the rupture.

#### Sorrento Primary School — Cumulative exposure times of different CO<sub>2</sub> concentrations

While the previous figures illustrated the spatial propagation of CO<sub>2</sub> concentrations, the following figures, Figures 8 to 10, delve into the cumulative exposure times for different concentrations. This information is helpful in understanding the potential for physiological impact and the temporal extent of the hazard zone. The figures display concentrations at a height of six feet above ground level.

Each figure illustrates the spread of a CO<sub>2</sub> for a single, specific concentration level. Within each figure, the color bands or contours display the cumulative exposure time for that particular concentration, revealing how long different areas were exposed to that exact concentration of CO<sub>2</sub>. For instance, the warm colors like red indicate longer exposure times, and cooler colors show shorter exposure times.

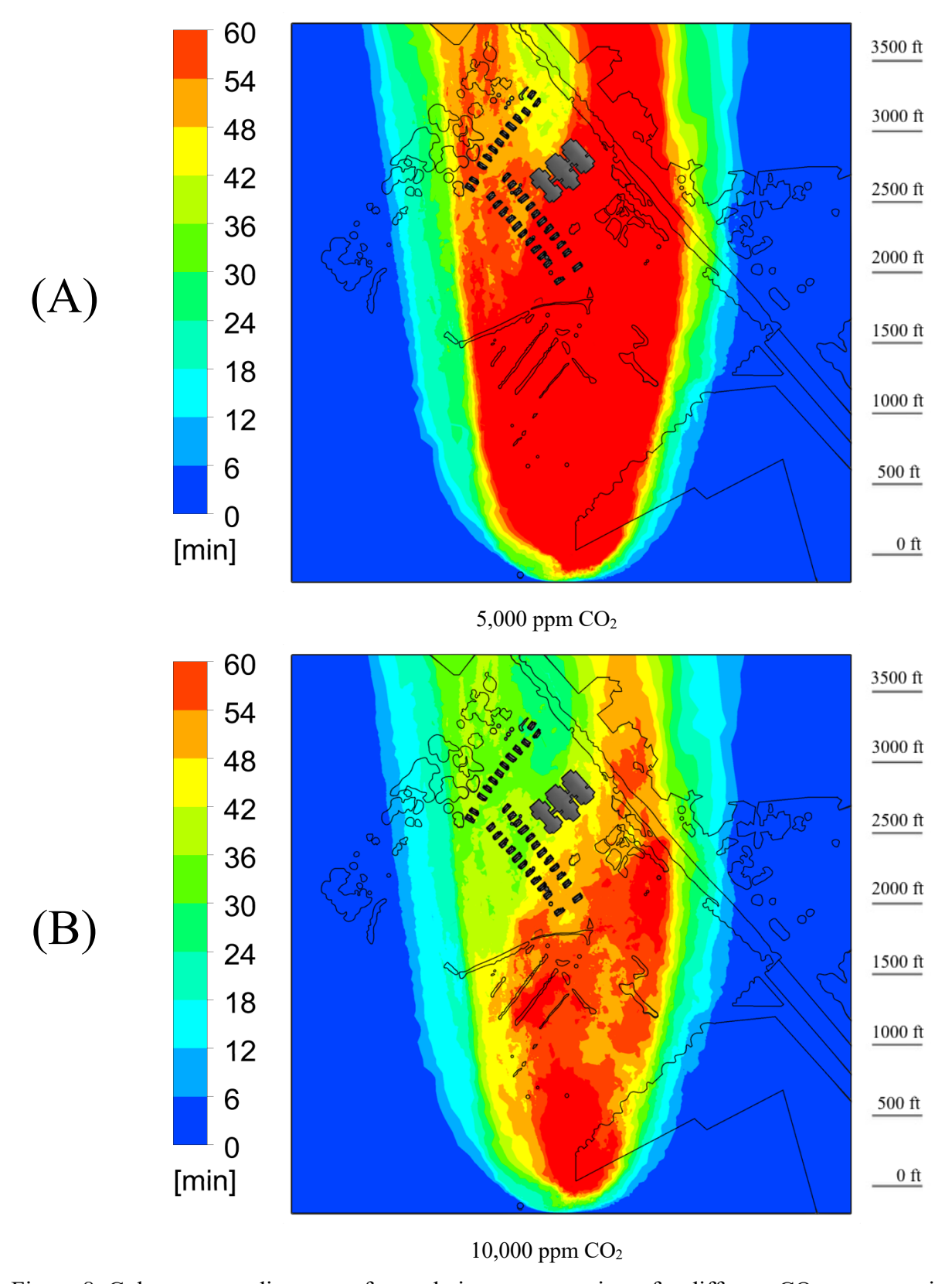


Figure 8. Color contour diagrams of cumulative exposure times for different CO<sub>2</sub> concentrations, for the Sorrento Primary School area, 5-minute shutoff time. (A) 5,000 ppm and (B) 10,000 ppm.

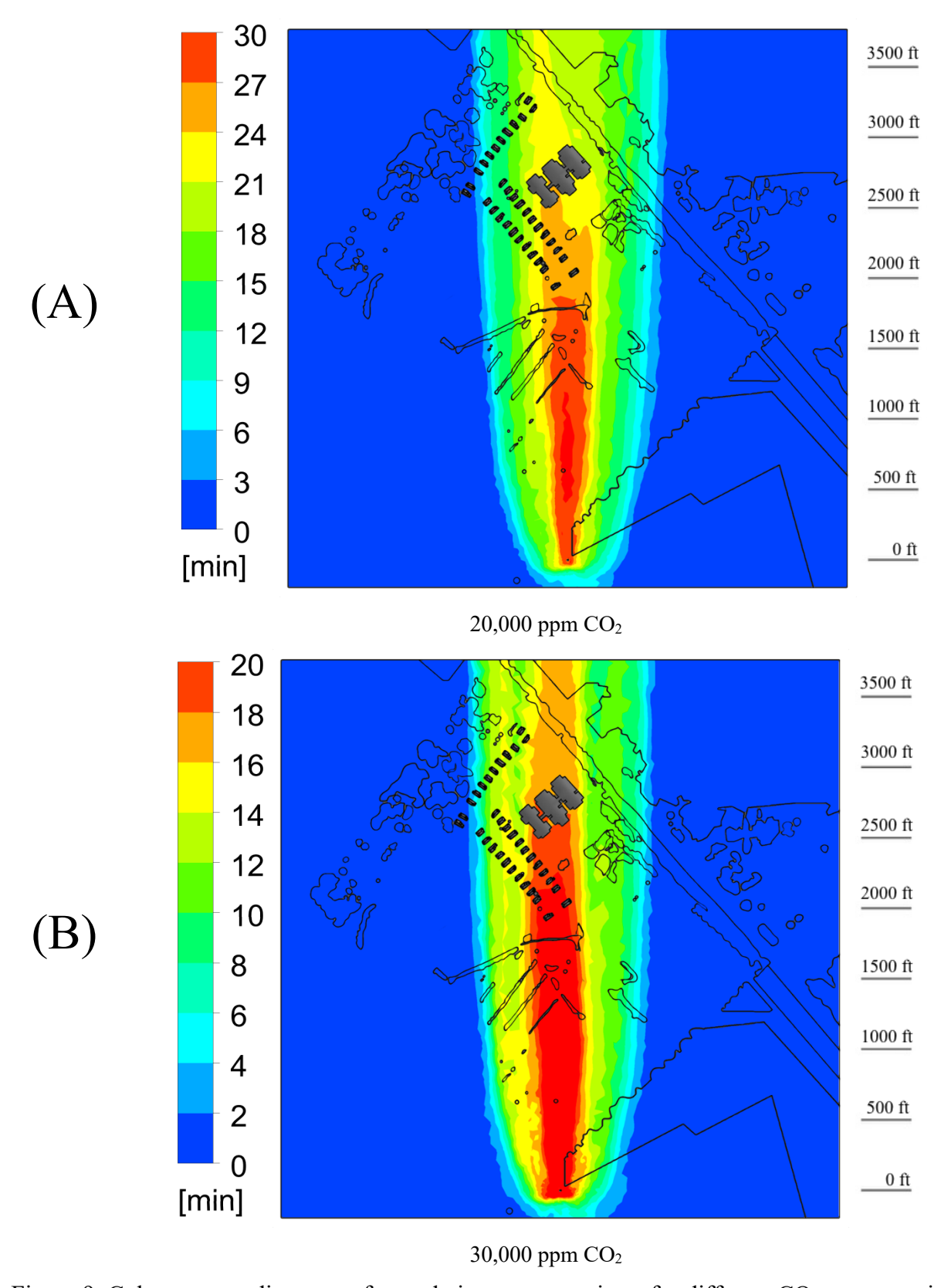


Figure 9. Color contour diagrams of cumulative exposure times for different CO<sub>2</sub> concentrations, for the Sorrento Primary School area, 5-minute shutoff time. (A) 20,000 ppm and (B) 30,000 ppm.

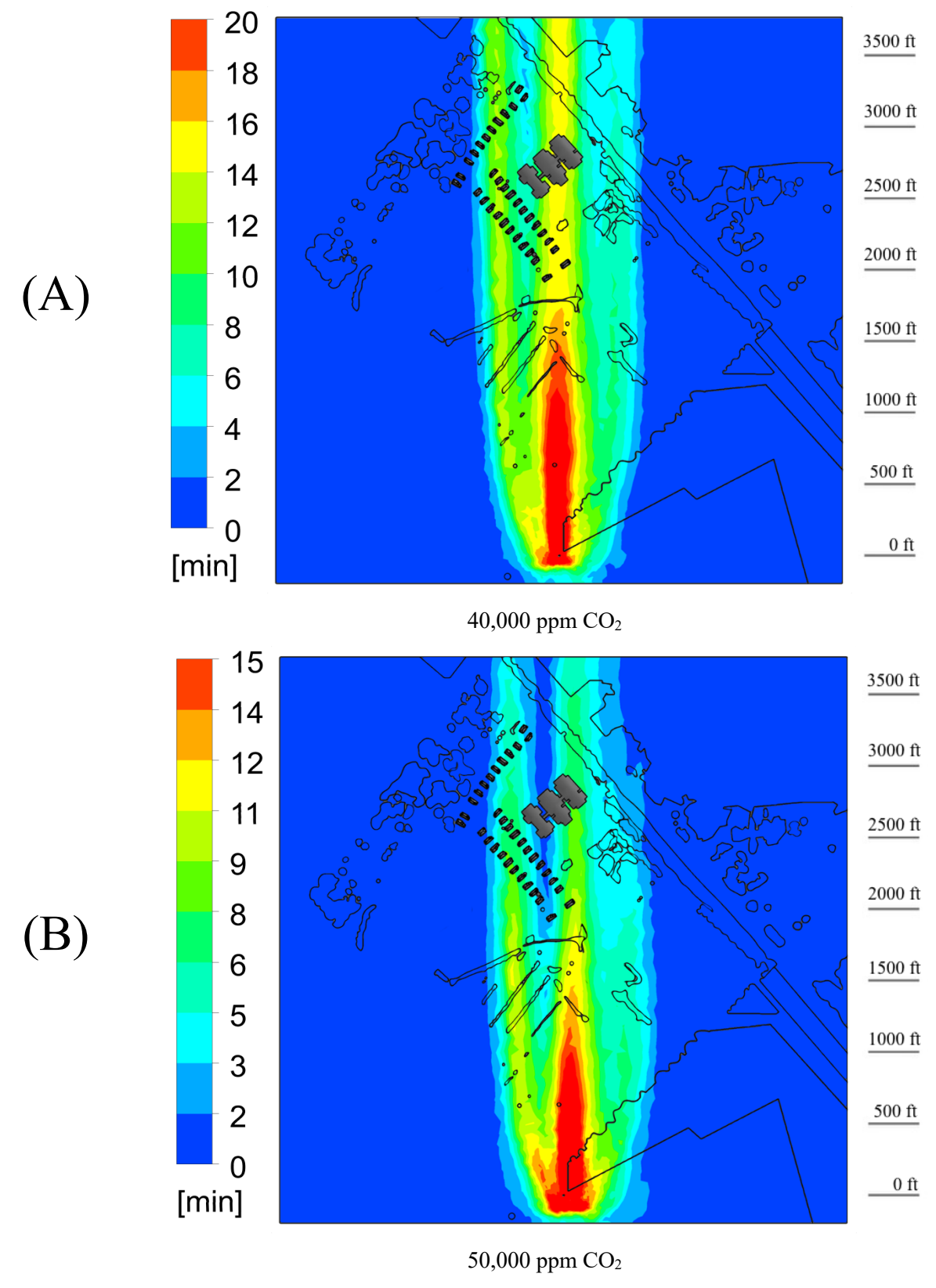


Figure 10. Color contour diagrams of cumulative exposure times for different CO<sub>2</sub> concentrations, for the Sorrento Primary School area, 5-minute shutoff time. (A) 40,000 ppm and (B) 50,000 ppm.

## Sorrento Primary School — Average CO<sub>2</sub> concentration

In addition to the color contour diagrams, the area-average concentration at a height of six feet, near the school, is graphed in Figure 11. The concentrations varied by 2% or less within a three-foot range, both above and below this height. While this graph does not capture the cumulative exposure experienced at this location, it is helpful for showing the average variation in CO<sub>2</sub> concentrations as a function of time. It is important to note that Figure 11 displays the average concentration values; different areas around the school are experiencing higher or lower concentrations of CO<sub>2</sub> at any given moment in time.

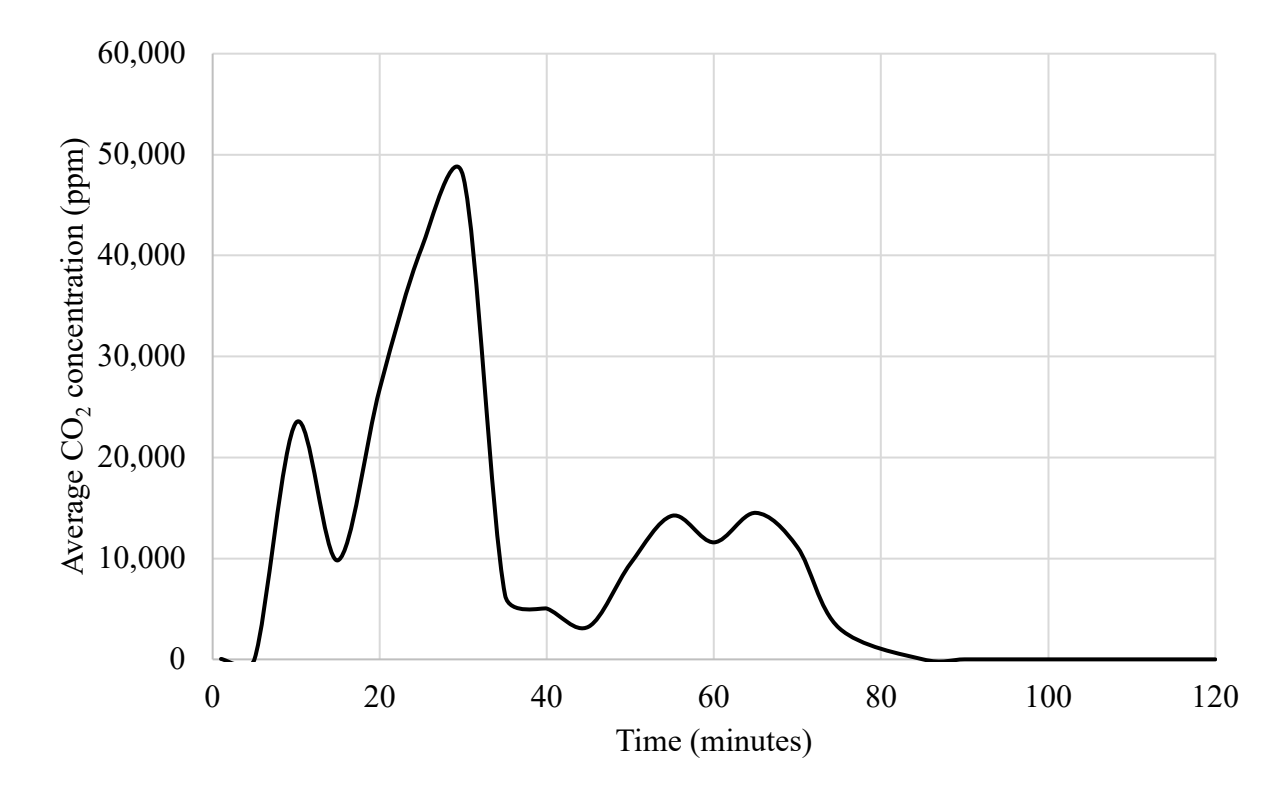


Figure 11. Average CO<sub>2</sub> concentration, in ppm, at the Sorrento Primary School as a function of time for a 5-minute shutoff time. The graph displays concentrations taken at a height of six feet. The concentrations varied by 2% or less within a three-foot range, both above and below this height.

#### Case 2 — 10-minute shutoff time

The second numerical model of the CO<sub>2</sub> pipeline rupture (with a 24-inch outer diameter and buried three feet underground) was run, simulating two hours of time after the initial rupture. Exactly ten minutes after the rupture began, the pipeline valves (located away from the rupture) were closed, and the remaining CO<sub>2</sub> in the pipeline exited into the atmosphere. The total amount of CO<sub>2</sub> released during the simulated rupture was approximately 19,200 barrels of CO<sub>2</sub> (which is the equivalent pre-rupture volume of pure CO<sub>2</sub> using the 42-gallon barrel, found from knowing the density and mass of CO<sub>2</sub>). For comparison, the 5-minute shutoff time resulted in an approximate 18,000 barrels of CO<sub>2</sub> being released. While the increase in volume of CO<sub>2</sub> released is due to the longer pipeline valve shutoff time, the maximum rate at which the CO<sub>2</sub> can exit the rupture is controlled by several factors, including the complex physical phenomena (such as phase change and choked flow) occurring at the rupture location.

Due to the complexity of the physical situation (time-varying changes in CO<sub>2</sub> concentrations over a large three-dimensional area), the results will be presented using several methods: (1) color contour figures of the CO<sub>2</sub> plume as it expands, (2) color contour figures showing the exposure times of different CO<sub>2</sub> concentrations over the area, (3) a graph showing the CO<sub>2</sub> concentration as a function time near the location of interest.

### Sorrento Primary School — Color contour images of the CO2 plume

The temporal evolution of the  $CO_2$  plume is captured in a series of qualitative diagrams, shown in Figures 12 to 17. These visualizations illustrate the plume's expansion, instantaneous concentrations (in ppm, *parts per million*), and dispersion patterns at key time intervals following the initial rupture. The figures display concentrations at a height of six feet above the ground. For the areas downstream of the rupture, around the Orange Grove Subdivision and Sorrento Primary School, the  $CO_2$  concentrations three feet above or below ( $\pm$  3 ft) the six-foot height can vary by up to 6 percent, depending on the time and location.

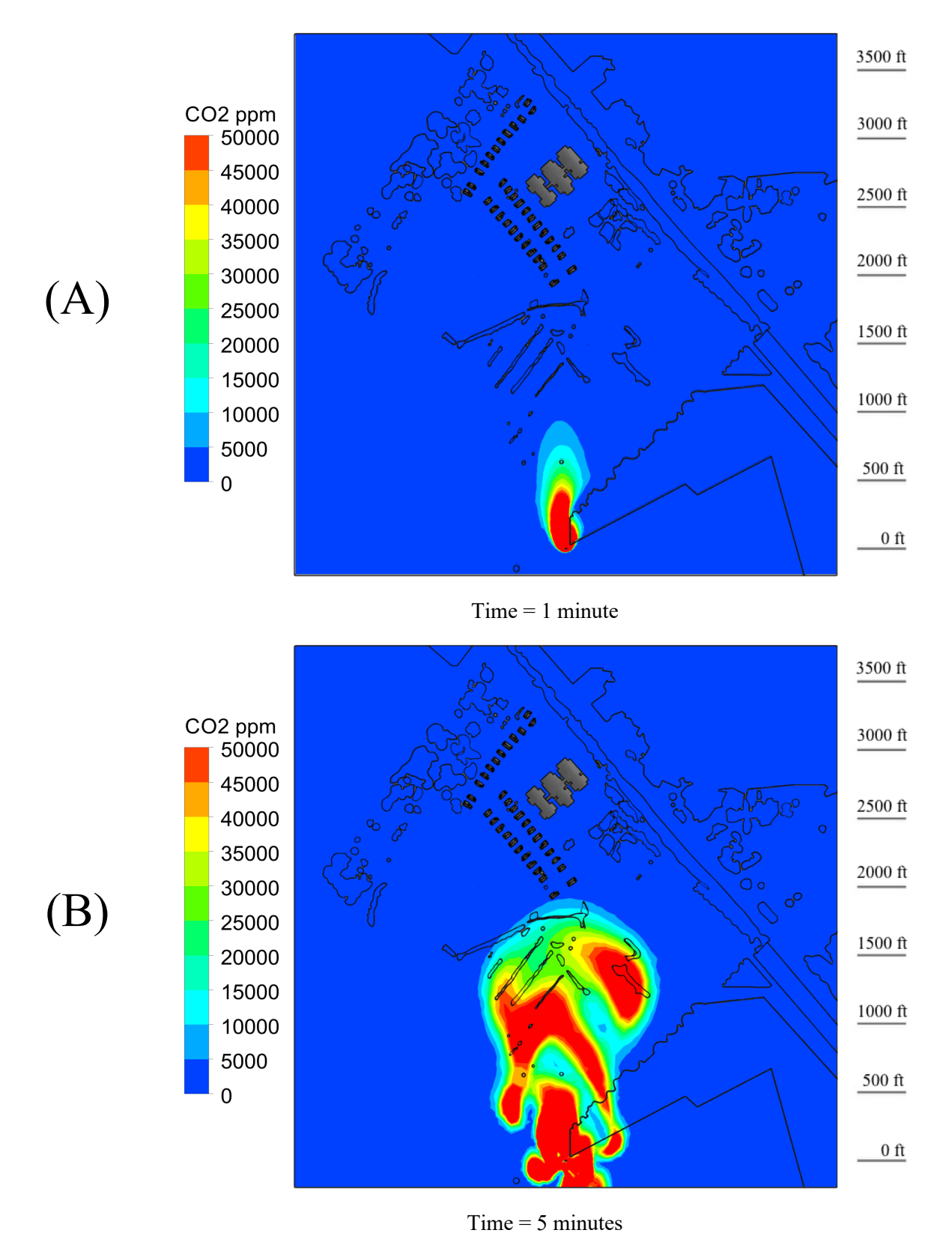


Figure 12. Contour diagrams of instantaneous CO<sub>2</sub> concentrations for the Sorrento Primary School area, 10-minute shutoff time. (A) 1 minute after the rupture and (B) 5 minutes after the rupture.

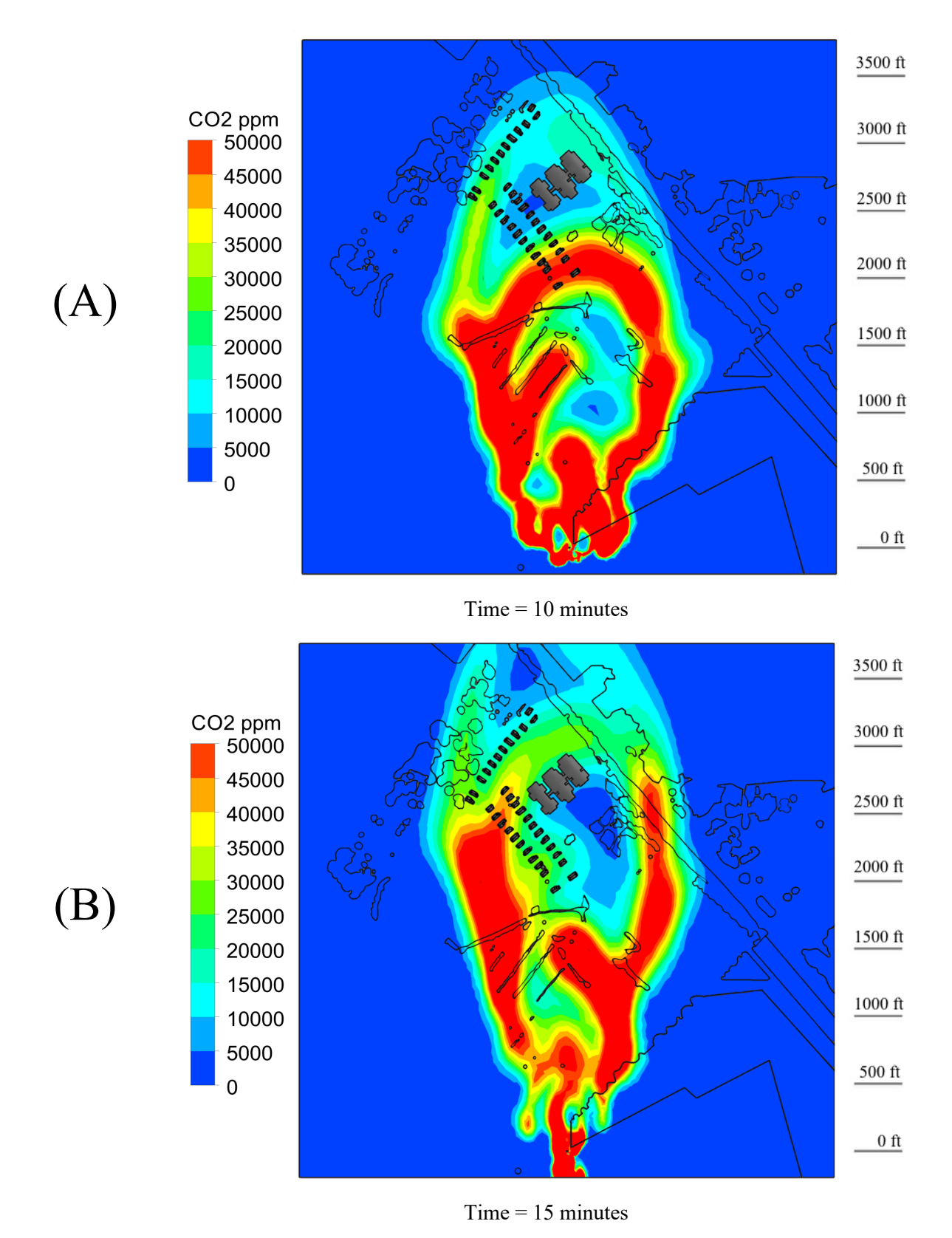


Figure 13. Contour diagrams of instantaneous CO<sub>2</sub> concentrations for the Sorrento Primary School area, 10-minute shutoff time. (A) 10 minutes after the rupture and (B) 15 minutes after the rupture.

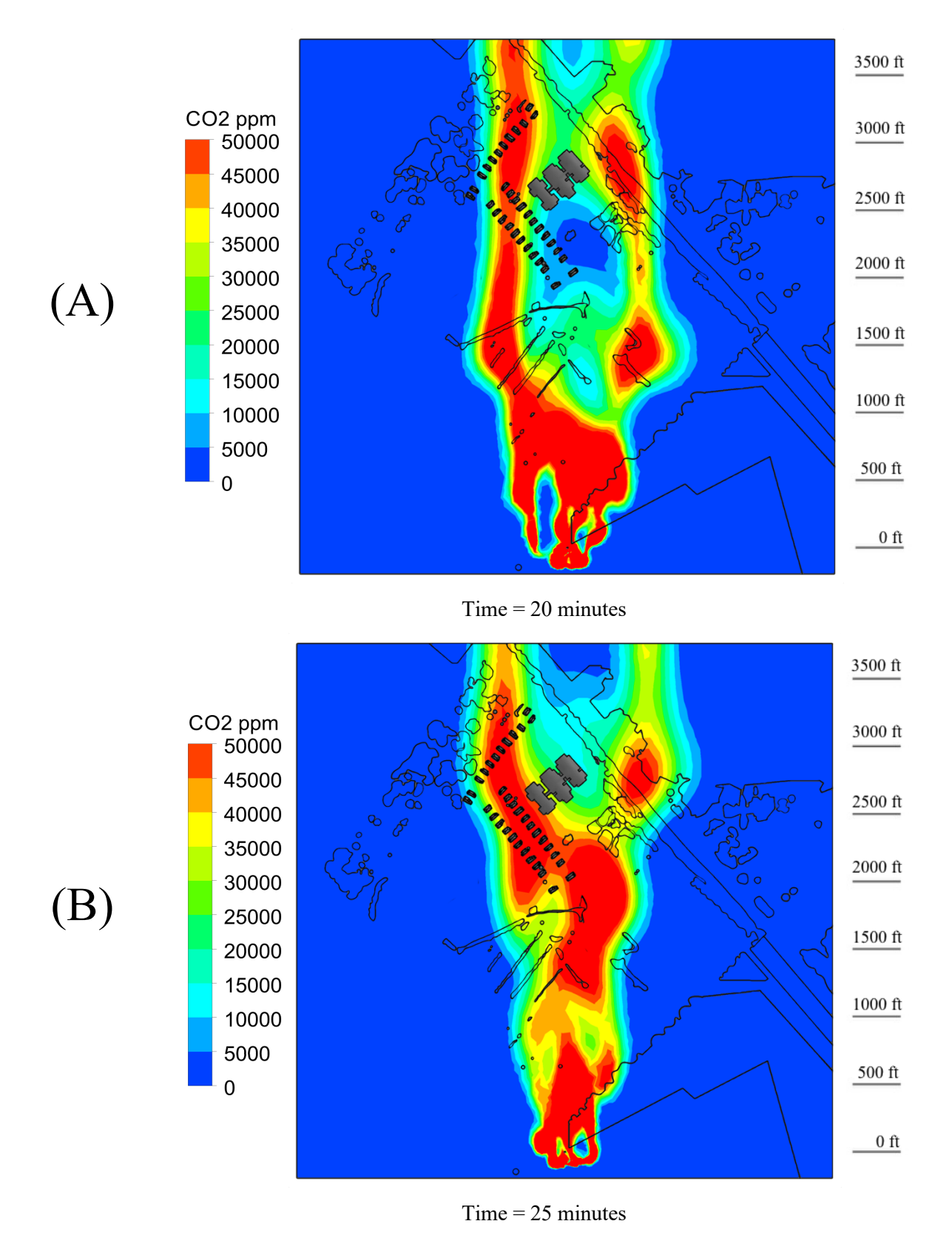


Figure 14. Contour diagrams of instantaneous CO<sub>2</sub> concentrations for the Sorrento Primary School area, 10-minute shutoff time. (A) 20 minutes after the rupture and (B) 25 minutes after the rupture.

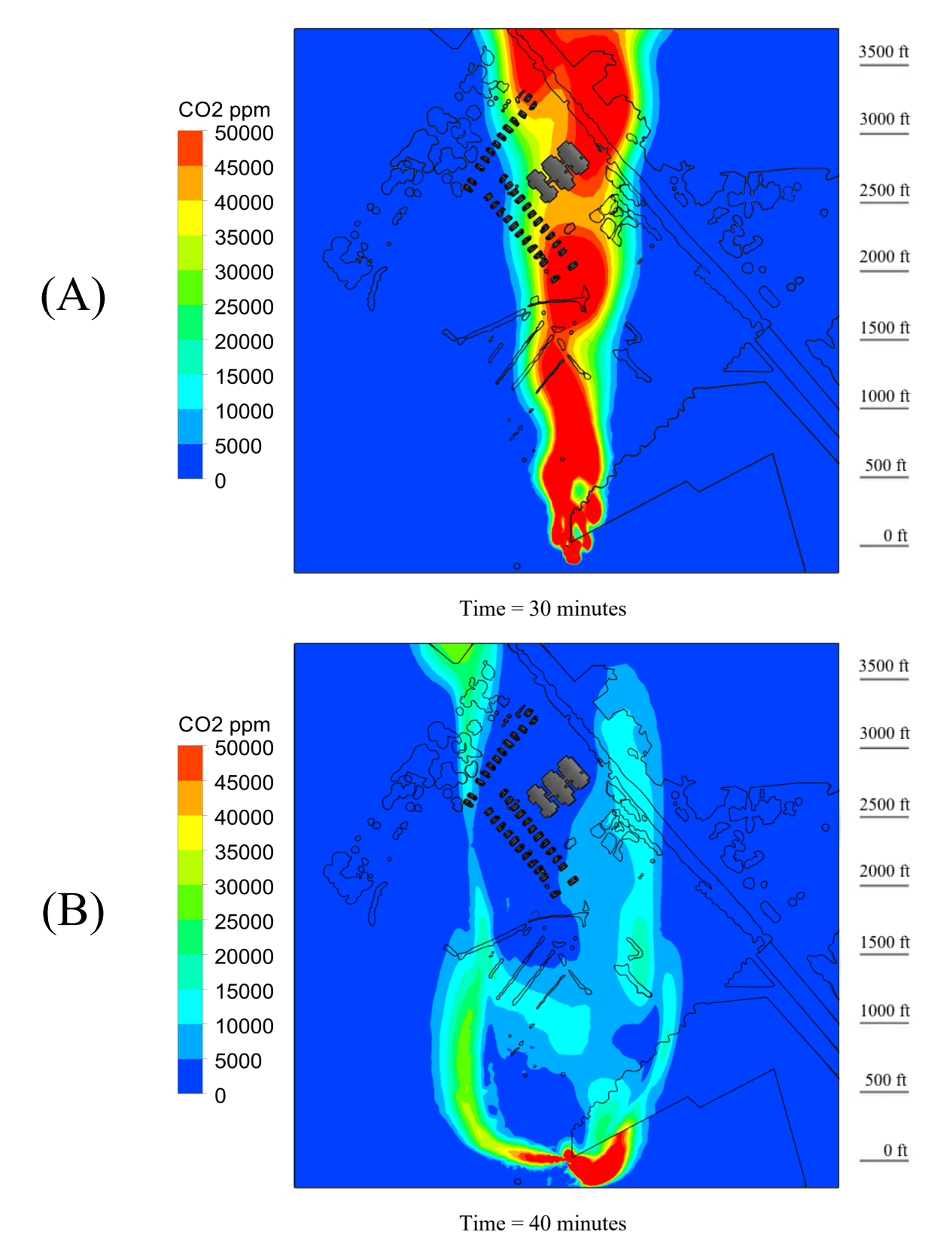


Figure 15. Contour diagrams of instantaneous CO<sub>2</sub> concentrations for the Sorrento Primary School area, 10-minute shutoff time. (A) 30 minutes after the rupture and (B) 40 minutes after the rupture.

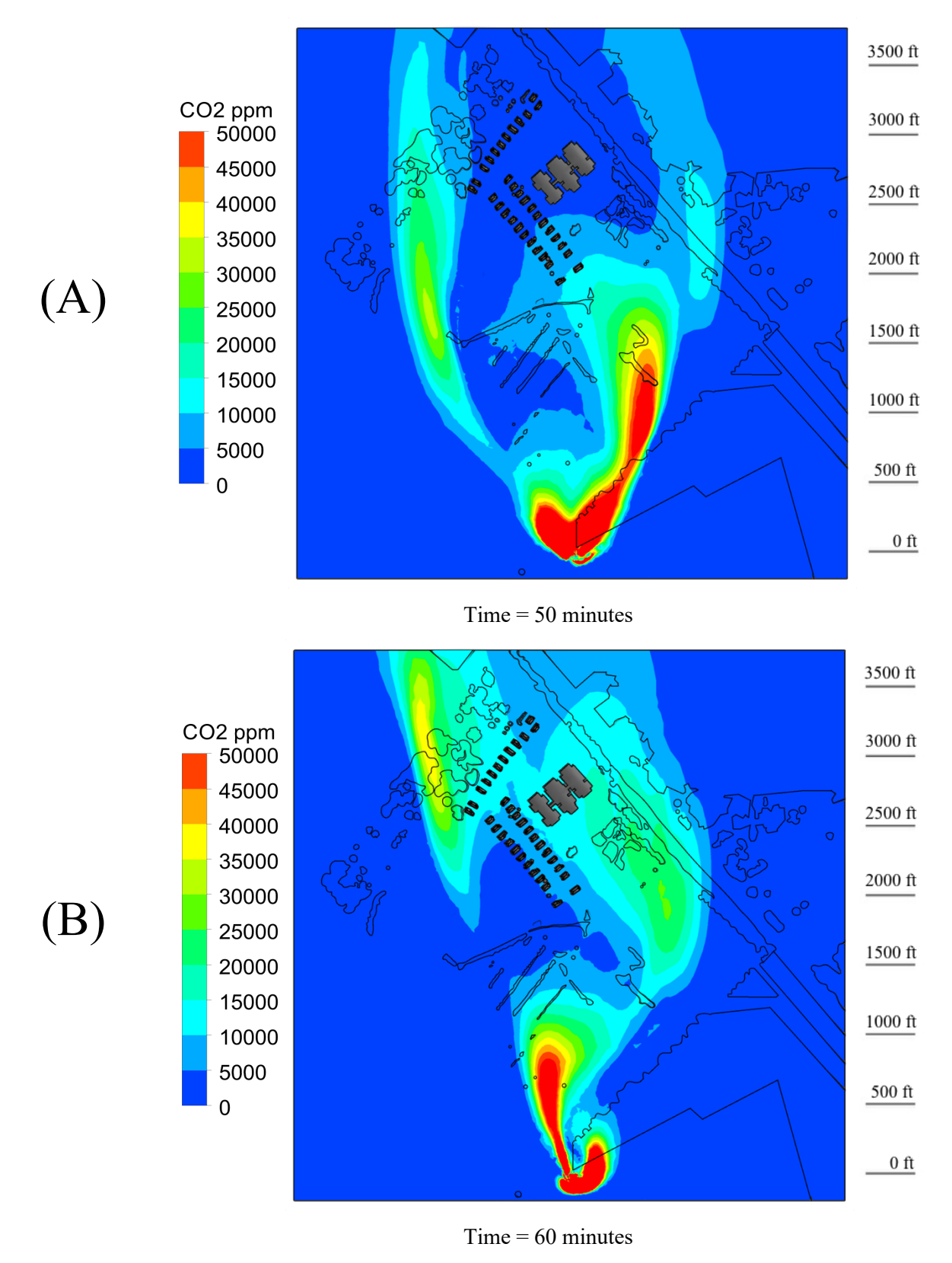


Figure 16. Contour diagrams of instantaneous CO<sub>2</sub> concentrations for the Sorrento Primary School area, 10-minute shutoff time. (A) 50 minutes after the rupture and (B) 60 minutes after the rupture.

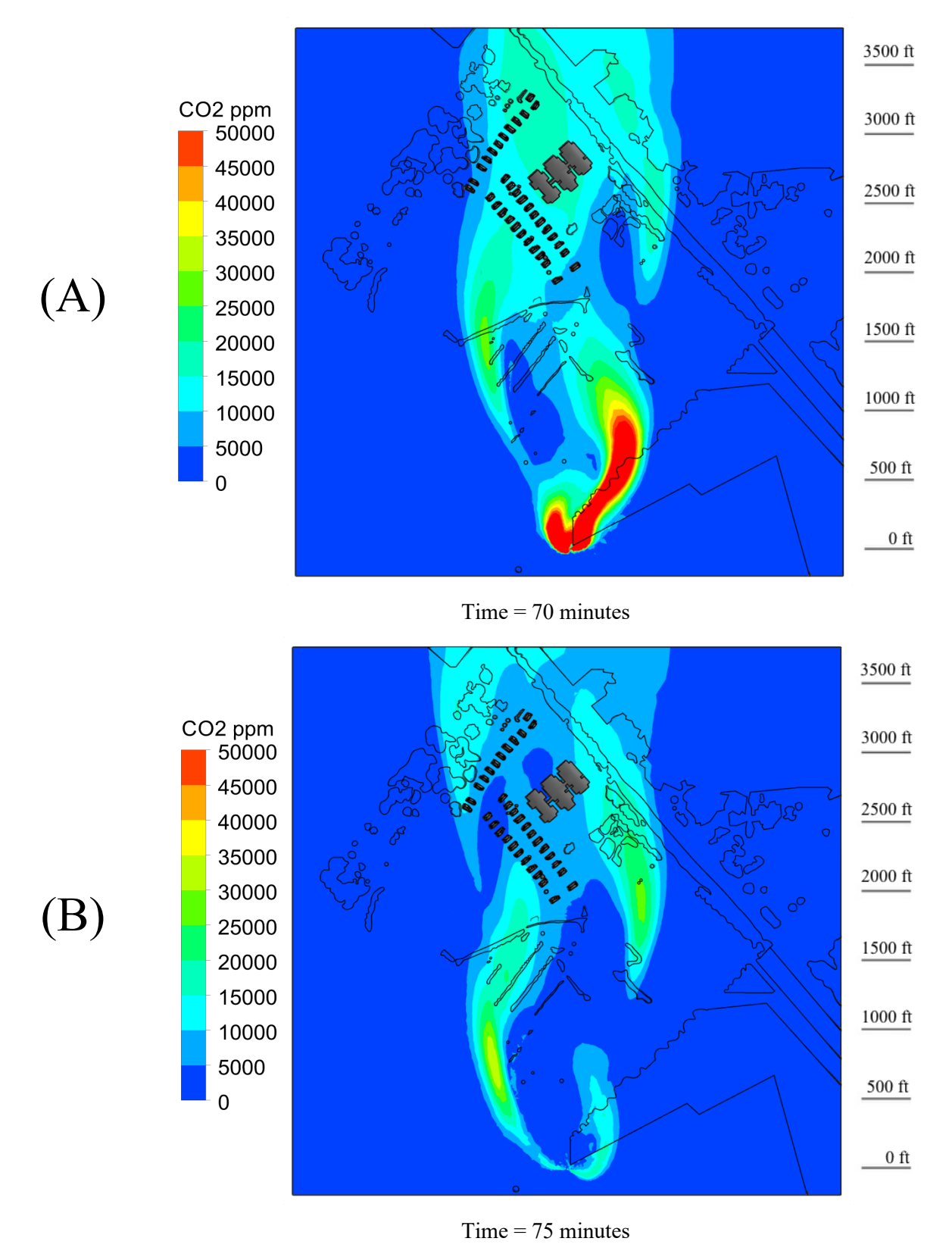


Figure 17. Contour diagrams of instantaneous CO<sub>2</sub> concentrations for the Sorrento Primary School area, 10-minute shutoff time. (A) 70 minutes after the rupture and (B) 75 minutes after the rupture.

#### Sorrento Primary School — Cumulative exposure times of different CO<sub>2</sub> concentrations

While the previous figures illustrated the spatial propagation of CO<sub>2</sub> concentrations, the following figures, Figures 18 to 20, delve into the cumulative exposure times for different concentrations. This information is helpful in understanding the potential for physiological impact and the temporal extent of the hazard zone. The figures display concentrations at a height of six feet above ground level.

Each figure illustrates the spread of a CO<sub>2</sub> for a single, specific concentration level. Within each figure, the color bands or contours display the cumulative exposure time for that particular concentration, revealing how long different areas were exposed to that exact concentration of CO<sub>2</sub>. For instance, the warm colors like red indicate longer exposure times, and cooler colors show shorter exposure times.

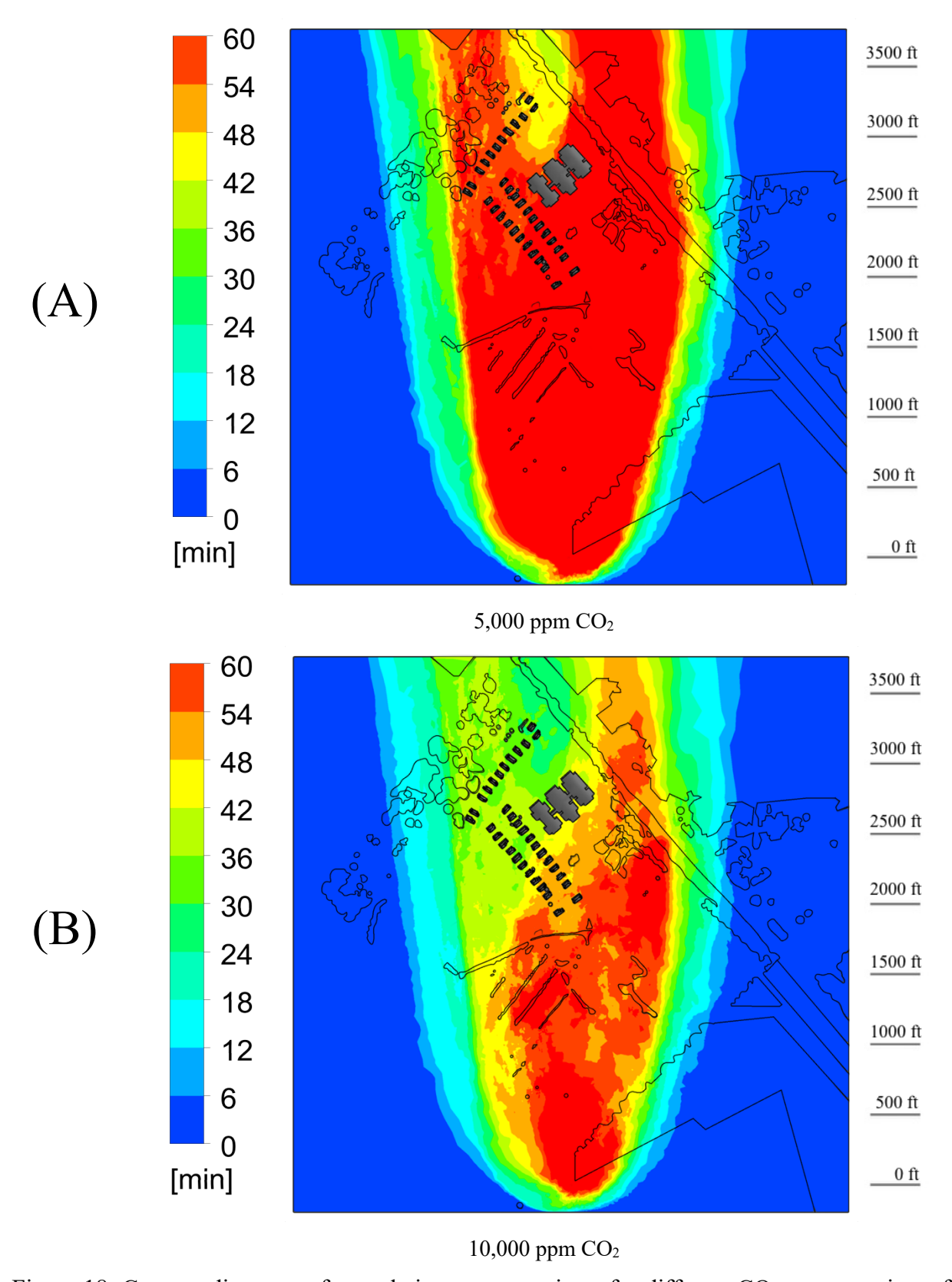


Figure 18. Contour diagrams of cumulative exposure times for different CO<sub>2</sub> concentrations, for the Sorrento Primary School area, 10-minute shutoff time. (A) 5,000 ppm and (B) 10,000 ppm.

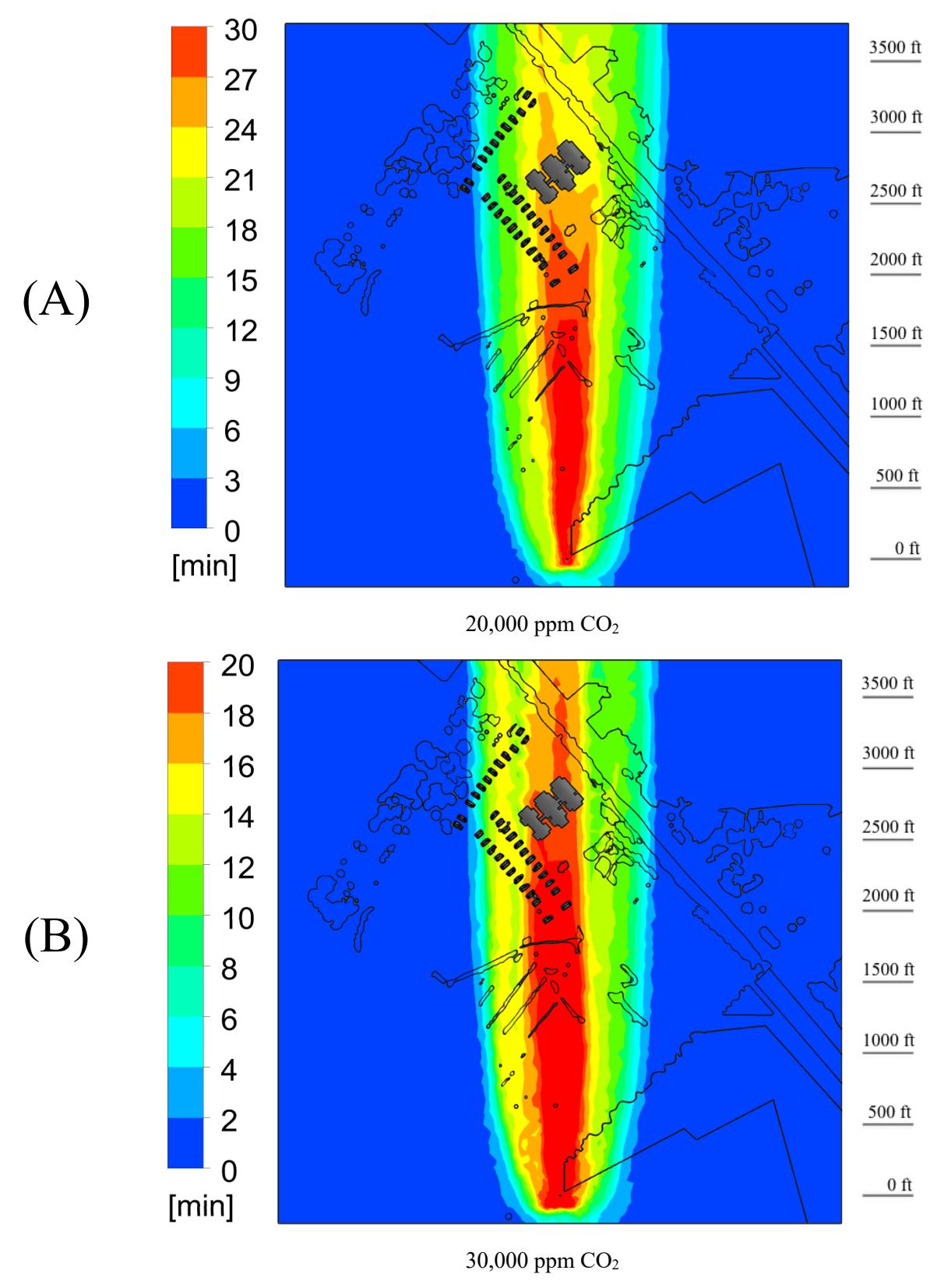


Figure 19. Contour diagrams of cumulative exposure times for different CO<sub>2</sub> concentrations, for the Sorrento Primary School area, 10-minute shutoff time. (A) 20,000 ppm and (B) 30,000 ppm.

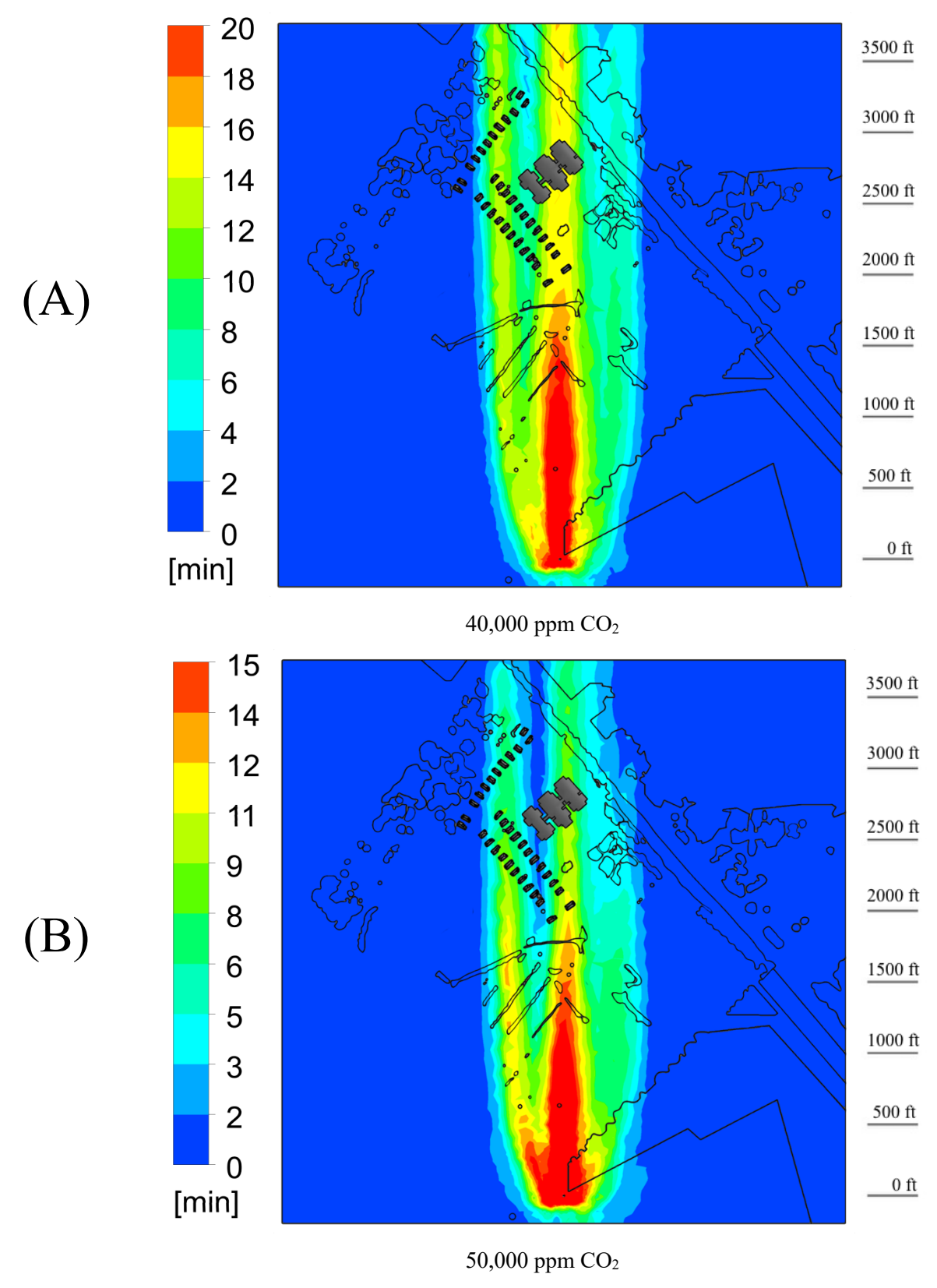


Figure 20. Contour diagrams of cumulative exposure times for different CO<sub>2</sub> concentrations, for the Sorrento Primary School area, 10-minute shutoff time. (A) 40,000 ppm and (B) 50,000 ppm.

#### Sorrento Primary School — Average CO<sub>2</sub> concentration

In addition to the color contour diagrams, the area-average concentration at a height of six feet, near the school, has been graphed in Figure 21. The concentrations varied by 2% or less within a three-foot range, both above and below this height. While this graph does not capture the cumulative exposure experienced at this location, it is helpful for illustrating the average variation in CO<sub>2</sub> concentrations over time. It is important to note that Figure 21 displays the average concentration values; different areas around the school are experiencing higher or lower concentrations of CO<sub>2</sub> at any given moment in time.

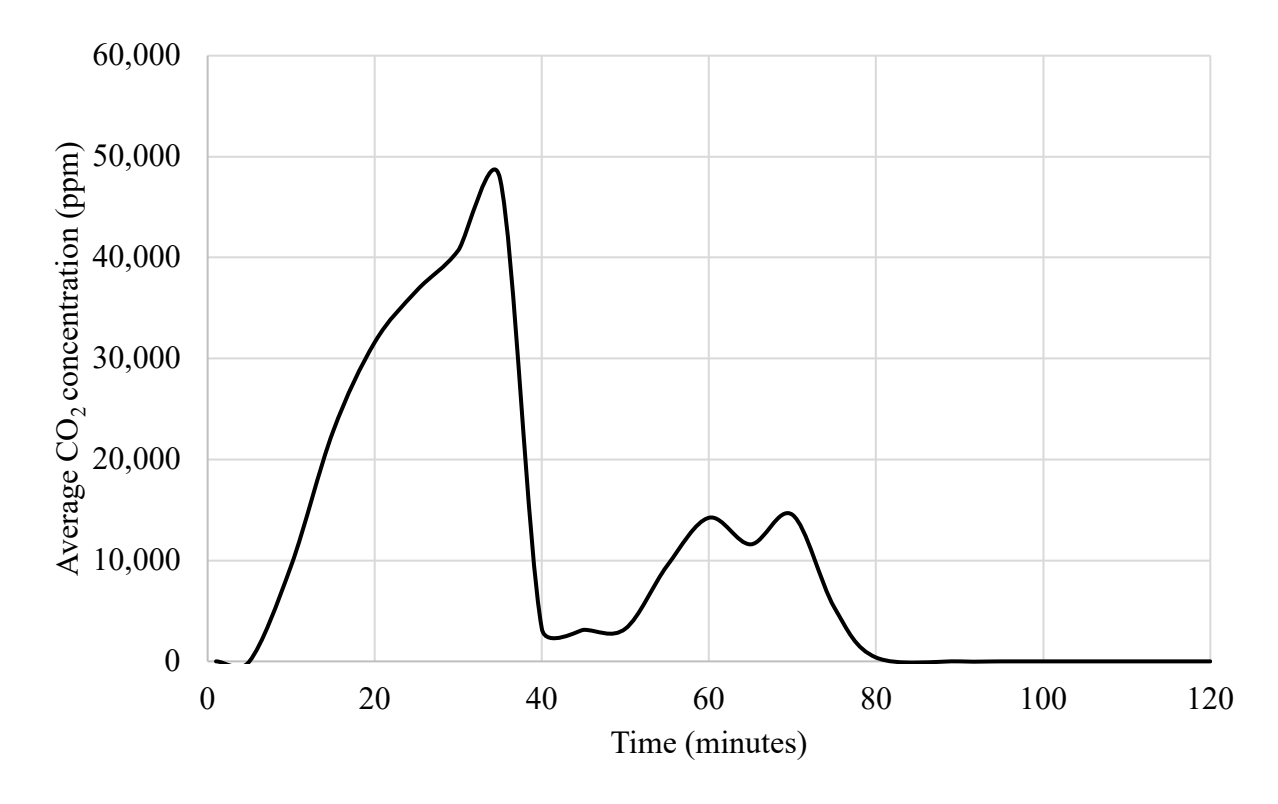


Figure 21. Average CO<sub>2</sub> concentration, in ppm, at the Sorrento Primary School as a function of time for a 10-minute shutoff time. The graph displays concentrations taken at a height of six feet. The concentrations varied by 2% or less within a three-foot range, both above and below this height.

#### **CONCLUDING REMARKS**

The purpose of this report is to investigate a pipeline rupture transporting carbon dioxide (CO<sub>2</sub>) and determine the resulting downstream CO<sub>2</sub> concentrations using computational fluid dynamics (CFD). The pipeline investigated here has a 24-inch outer diameter and was buried three feet underground. The rupture was a guillotine cut located near the Sorrento Primary School and the Orange Grove Subdivision. It was conservatively assumed that the rupture would be detected and the valves closed exactly five or ten minutes after the rupture occurred. The numerical model was run to simulate the two hours following the pipeline rupture, in order to determine the resulting downstream CO<sub>2</sub> concentrations.

The case with the longer shutoff time (Case 2, ten minutes) resulted in a larger amount of CO<sub>2</sub> being released. The ten-minute shutoff time increased the predicted cumulative exposure times by a few minutes in regions further downstream from the rupture. For example, comparing Figure 10(B) with Figure 20(B), the trailing edge of the 15-minute 50,000 ppm CO<sub>2</sub> concentration is approximately 375 ft further downstream from the rupture. The longer shutoff time also affected the average concentration of CO<sub>2</sub> near the Sorrento Primary School, as shown in Figures 11 and 21, resulting in visibly higher values between 15 and 35 minutes after the rupture.

The CO<sub>2</sub> plume and concentration results from the CFD simulation are sensitive to the initial input parameters. The output is significantly influenced by variables such as the location of the rupture, atmospheric conditions (including wind speed), terrain, time to detect a leak and close the valves, and the characteristics of the pipe rupture. Variations in these inputs can produce markedly different outcomes for CO<sub>2</sub> plume dispersion, leading to large increases or decreases in the predicted CO<sub>2</sub> concentrations at specific locations and times.

Multiple factors affect the CO<sub>2</sub> plume's concentration, size, and trajectory. During a high-pressure rupture, factors such as high density, buoyancy, and atmospheric conditions combine to create a denser-than-air cloud that can accumulate in low-lying areas. Upon rupture, the CO<sub>2</sub> expands rapidly, creating a cold, dense, multiphase plume that behaves distinctly from a release of low-pressure gas.

#### Some key factors affecting CO<sub>2</sub> dispersion:

## **Density and buoyancy**

- **High density:** At standard temperature and pressure, CO<sub>2</sub> is denser than dry air. When a high-pressure CO<sub>2</sub> pipeline ruptures, the resulting gas cools and expands, and this dense (denser than air), cold gas sinks toward the ground.
- **Buoyancy effects:** The behavior of the CO<sub>2</sub> plume is heavily influenced by buoyancy in low winds. The initial release is very cold due to rapid depressurization, causing it to be denser than the surrounding air. It creates a plume that stays low to the ground and displaces the existing oxygen.
- **Temperature:** In a pipeline rupture, due to several physical processes, the emerging CO<sub>2</sub> is colder than the ambient, causing the plume to sink. As the cold CO<sub>2</sub> plume is warmed by the ground and ambient air, its buoyancy changes, which affects how it mixes.

#### **Atmospheric conditions**

- Wind speed and turbulence: Wind is a critical factor in dispersing the CO<sub>2</sub> plume. Higher wind speeds enhance mixing and help to dilute the plume faster. Under low wind speed or calm conditions, the CO<sub>2</sub> plume can remain concentrated and accumulate, particularly in low-lying areas and confined spaces.
- Unsteady wind gusts: While a steady wind direction moves the entire plume downwind, gusts can alter the plume's shape, path, and concentration in complex ways that are difficult to predict.
  - O Directional shift: Gusts, which are sudden changes in wind speed and direction, can cause the plume to "snake" or oscillate. This means the hazardous plume's path is not a straight line downwind but instead can shift horizontally, affecting a wider or different area than a steady wind would.
  - Rapid advection: Strong gusts can quickly transport pockets of concentrated CO<sub>2</sub> to new areas, potentially affecting people farther away from the rupture site than would be expected under calm conditions.
  - Temporary concentration spikes: While overall mixing can increase, a wind gust can temporarily concentrate the plume in a specific location before it disperses, potentially creating temporary "hotspots" of higher CO<sub>2</sub> concentration. This is particularly true for dense gas plumes that are already prone to accumulation.

- **Atmospheric stability:** The stability of the atmosphere (how prone it is to vertical motion) affects how gases disperse.
  - Unstable atmosphere (e.g., sunny day): A hot ground surface causes air to rise,
     creating turbulence that promotes good vertical mixing and dilution.
  - Stable atmosphere (e.g., clear night): A cold ground surface causes air to be stable and resist vertical movement. This can trap a heavy CO<sub>2</sub> plume near the ground surface.
- **Temperature inversions:** This is when a layer of cooler air near the ground is trapped under a layer of warmer air above it. This could help trap a layer of colder, dense CO<sub>2</sub> near the ground, preventing it from mixing vertically.

### **Topography**

- Terrain features: Hills, valleys, and other topographical features can have a major impact on dispersion. A dense CO<sub>2</sub> plume can flow and accumulate in low-lying areas, like valleys, gullies, displacing the oxygen in that space and creating a major hazard.
- **Urban areas:** Buildings and urban structures can create "urban canyons" that affect airflow, reduce ventilation, and trap gases like CO<sub>2</sub>.

## Effect of initial pipeline pressure

A higher initial pipeline pressure directly impacts the potential severity of a CO<sub>2</sub> pipeline rupture.

- **Increased mass flow rate:** Higher pressure forces more fluid through the rupture, resulting in a higher initial flow rate.
- Greater release: Higher pressure means the CO<sub>2</sub> is in a denser, supercritical state, so more mass is contained within a given pipe volume. A rupture will therefore release a larger total mass of CO<sub>2</sub>.
- Larger and denser cloud: The rapid depressurization from a higher pressure causes more intense cooling. The resulting cold, dense CO<sub>2</sub> cloud has a greater volume and lower temperature, which increases the likelihood of it remaining near the ground and spreading further.

#### Effect of pipe length

The length of the pipe segment between isolation valves is a critical determinant of the total volume of CO<sub>2</sub> released.

- Venting volume: A pipeline rupture typically results in the release of CO<sub>2</sub> from the two nearest isolation valves, one on either side of the rupture. The volume of CO<sub>2</sub> in this "venting segment" is proportional to the pipeline length. A longer pipe segment between valves contains a significant amount of stored, high-pressure CO<sub>2</sub>.
- Release duration: A longer pipe segment means a larger mass of CO<sub>2</sub> to be released, so the high-flow discharge phase lasts longer than it would for a shorter segment.

#### Effect of delays in closing pipeline valves

Delays in isolating the ruptured section have major consequences for the overall CO<sub>2</sub> release and the duration of the hazard.

- Increased total release: The longer the valves remain open, the more CO<sub>2</sub> is released. This increases the total volume of CO<sub>2</sub>, expanding the size and duration of the plume.
- **Hazard duration:** A delay in valve closure directly prolongs the duration of the release and the time it takes for the CO<sub>2</sub> concentration to drop to safe levels.
- **Impact on plume dispersion:** A longer release period allows the CO<sub>2</sub> plume to be carried further away by wind, potentially affecting a larger area.

## Effect of impurities in a CO<sub>2</sub> pipeline

The presence and concentration of impurities (such as water, nitrogen, oxygen, sulfur oxides, nitrogen, and hydrogen sulfide, etc.) vary depending on the CO<sub>2</sub> source and the capture technology used. Impurities in the CO<sub>2</sub> pipeline can impact the consequences of a rupture by altering the physical behavior of the released fluid, the size and nature of the resulting plume, and the potential toxicity of the immediate environment.

- Modified Phase Behavior: Impurities change the critical point, and phase change temperature and pressure, of the CO<sub>2</sub> mixture, altering how it behaves during rapid decompression.
- Altered Dispersion Rate: The presence of impurities can make the released plume less
  dense than pure in some scenarios, potentially allowing it to mix with the atmosphere and
  disperse faster, or conversely, alter its buoyancy.
- Increased Health Risks: Many potential impurities, such as hydrogen sulfide or sulfur dioxide, are highly toxic at lower concentrations and could lead to severe health risks beyond the hazard of a CO<sub>2</sub> plume.

#### REFERENCES

[1] Food Safety and Inspection Service, Carbon Dioxide Health Hazard Information Sheet, Aug. 2020, <a href="https://www.fsis.usda.gov/sites/default/files/media\_file/2020-08/Carbon-Dioxide.pdf">https://www.fsis.usda.gov/sites/default/files/media\_file/2020-08/Carbon-Dioxide.pdf</a>

[2] Air Products Blue Energy LLC Joint Permit Application ("JPA"), Attach. 2-02a La. Public Trust Doctrine Analysis, Oct. 03, 2025,

https://sonlite.dnr.state.la.us/dnrservices/redirectUrl.jsp?dID=15370940.

[3] U.S. Department of Transportation, Pipeline and Hazardous Materials Safety Administration. Failure Investigation Report - Denbury Gulf Coast Pipelines, LLC - Pipeline Rupture/Natural Force Damage. May 26, 2022,

https://www.phmsa.dot.gov/sites/phmsa.dot.gov/files/2024-06/Failure-Investigation-Report-Denbury-Gulf-Coast-Pipeline.pdf.

[4] Iowa Environmental Mesonet (IEM), Iowa State University. *REG Station Information*. Retrieved July 2025,

https://www.mesonet.agron.iastate.edu/sites/site.php?station=REG&network=LA\_ASOS.

[5] U.S. Department of Transportation, Pipeline and Hazardous Materials Safety Administration. "Valve Rule Fact Sheet." 5 Oct. 2022, https://www.phmsa.dot.gov/rulemaking-implementation/valve-rule/valve-rule-fact-sheet.

[6] Pipeline and Hazardous Materials Safety Administration (PHMSA), Department of Transportation. "Pipeline Safety: Requirement of Valve Installation and Minimum Rupture Detection Standards" (Final Rule). *Federal Register*, Vol. 87, No. 68, April 8, 2022, pp. 20940, 20950, https://www.federalregister.gov/documents/2022/04/08/2022-07133/pipeline-safety-requirement-of-valve-installation-and-minimum-rupture-detection-standards

[7] Sorrento Primary School. Google Maps, Retrieved July 2025,

https://www.google.com/maps/place/Sorrento+Primary+School/@30.1549293,-

90.885887,1230m/data=!3m1!1e3!4m6!3m5!1s0x8626cb198d14b173:0xb22b864c53269aa9!8m 2!3d30.1569726!4d-

90.8855281!16s%2Fg%2F1262gn8c8!5m1!1e4?entry=ttu&g\_ep=EgoyMDI1MDkyNC4wIKXM DSoASAFQAw%3D%3D.

- [8] J. Abraham, L. Cheng, J.M. Gorman, CFD Simulation Models and Diffusion Models for Predicting Carbon Dioxide Plumes following Tank and Pipeline Ruptures—Laboratory Test and a Real-World Case Study. Energies 17 (2024) 1079.
- [9] F. Menter, Two-equation Eddy-viscosity turbulence models for engineering applications, AIAA J. 32 (8) (1994) 1598–1605.
- [10] F. Menter, Review of the shear-stress transport turbulence model experience from an industrial perspective, Int. J. Comput. Fluid. D. 23 (4) (2009) 305–316.
- [11] U. Engdar, J. Klingmann, Investigation of two-equation turbulence models applied to a confined axis-symmetric swirling flow, in: ASME 2002 Pressure Vessels and Piping Conference, (2002) 199–206.
- [12] A. Li, X. Chen, L. Chen, R. Gao, Study on local drag reduction effects of wedge-shaped components in elbow and T-junction close-coupled pipes, Build. Simul. 7 (2) (2014)175–184.
- [13] Y. Bayazit, E.M. Sparrow, D.D. Joseph, Perforated plates for fluid management: plate geometry effects and flow regimes, Int. J. Therm. Sci. 85 (2014) 104–111.
- [14] J. Park, S. Park, P.M. Ligrani, Numerical predictions of detailed flow structural characteristics in a channel with angled rib turbulators, J. Mech. Sci. Technol. 29 (11) (2015) 4981–4991.
- [15] W. Li, J. Ren, J. Hongde, Y. Luan, P. Ligrani, Assessment of six turbulence models for modeling and predicting narrow passage flows, part 2: pin fin arrays, Numer. Heat. Tr. A Appl. 69 (2016) 445–463.
- [16] J.M. Gorman, E.M. Sparrow, J.P. Abraham, W.J. Minkowycz, Evaluation of the efficacy of turbulence models for swirling flows and effect of turbulence intensity on heat transfer, Numer. Heat. Tr. B Fund. 70 (6) (2016) 485–502.
- [17] E.M. Sparrow, J.M. Gorman, J.P. Abraham, W.J. Minkowycz, Validation of turbulence models for numerical simulation of fluid flow and convective heat transfer, Adv. Heat Tran. 49 (2017) 1–35.
- [18] D.B. Bryant, E.M. Sparrow, J.M. Gorman, Turbulent pipe flow in the presence of centerline velocity overshoot and wall-shear undershoot, Int. J. Therm. Sci. 125 (2018) 218–230.
- [19] Y. Hesheng, T. Jesse, Validation and optimization of SST k-ω turbulence model for pollutant dispersion within a building array, Atmos. Environ. 145 (2016) 225–238.

- [20] P.J. Richards, S.E. Norris, Appropriate boundary conditions for computational wind engineering models revisited. Journal of Wind Engineering and Industrial Aerodynamics, 99(4) (2011) 257-266.
- [21] J. Wieringa, Updating the Davenport roughness classification. Journal of Wind Engineering and Industrial Aerodynamics, 41(1-3) (1992) 357-368.
- [22] J.M. Gorman, E.M. Sparrow, S.D.M. Katz, W.J. Minkowycz, Convective heat transfer coefficients on all external surfaces of a generic residential building in crossflow. Numerical Heat Transfer, Part A: Applications, 75(2) (2019) 71-90.